Article:
Shi, Y-G, Zhu, C-M, Li, D-H et al. (6 more authors) (2021) New Horizons in Microbiological Food Safety: Ultraefficient Photodynamic Inactivation Based on a Gallic Acid Derivative and UV-A Light and Its Application with Electrospun Cyclodextrin Nanofibers. Journal of Agricultural and Food Chemistry, 69 (49). pp. 14961-14974. ISSN 0021-8561

https://doi.org/10.1021/acs.jafc.1c04827

New Horizons in Microbiological Food Safety: Ultra-efficient Photodynamic Inactivation Based on a Gallic Acid Derivative and UV-A Light and Exploring a Salient Application with Electrospun Cyclodextrin Nanofibers

Journal:	*Journal of Agricultural and Food Chemistry*
Manuscript ID	Draft
Manuscript Type:	Article
Date Submitted by the Author:	n/a
Complete List of Authors:	Shi, Yugang; Zhejiang Gongshang University, School of Food Science and Biotechnology Zhu, Chen-min; Zhejiang Gongshang University, School of Food Science and Biotechnology Li, Dong-hui; Institute of Food Microbiology, School of Food Science and Biotechnology Shi, Ze-yu; Zhejiang Shuren University Gu, Qing; Institute of Food Microbiology, School of Food Science and Biotechnology Chen, Yue-wen; Institute of Food Microbiology, School of Food Science and Biotechnology Wang, Jie-qian; Institute of Food Microbiology, School of Food Science and Biotechnology Ettelaie , Rammile; University of Leeds Chen, Jian-she; Zhejiang Gongshang University, School of Food Science and Biotechnology

Submit online to *Journal of Agricultural and Food Chemistry*

Manuscript Number:

Title

New Horizons in Microbiological Food Safety: Ultra-efficient Photodynamic Inactivation Based on a Gallic Acid Derivative and UV-A Light and Exploring a Salient Application with Electrospun Cyclodextrin Nanofibers

Yu-gang Shi [a,b]*, Chen-min Zhu [a], Dong-hui Li [a,b], Ze-yu Shi [c], Qing Gu [a,b], Yue-wen Chen [a,b], Jie-qian Wang, Rammile Ettelaie [d]

[a] School of Food Science and Biotechnology, Zhejiang Gongshang University, Hangzhou, Zhejiang 310035, China

[b] Institute of Food Microbiology, Zhejiang Gongshang University, Hangzhou, Zhejiang 310035, China

[c] College of Biology and Environmental Engineering, Zhejiang Shuren University, Hangzhou 310015, China

[d] School of Food Science and Nutrition, University of Leeds, Leeds, LS2 9JT, UK

Corresponding Author:

Yu-gang Shi

School of Food Science and Biotechnology, Zhejiang Gongshang University, Xiasha University Town, Xuezheng Str. 18, Hangzhou 310018, China

Tel.: 86-0571-28008927

E-mail: yugangshi@zjgsu.edu.cn

ABSTRACT

The excellent bactericidal effect of octyl gallate (OG)-mediated photodynamic inactivation (PDI) against foodborne pathogens (*Escherichia coli* and *Staphylococcus aureus*) was evaluated in relation to the mode of action. UV-A irradiation (wavelength, 365 nm; irradiance, 8.254±0.18 mW/cm^2) of the bacterial suspension containing 0.15 mM OG could lead to a >5-Log reduction of viable cell counts within 30 min for *E. coli*, and only 5 min for *S. aureus*, respectively. Reactive oxygen species (ROS) formation was considered as the main reason for the bactericidal effect of OG+UV-A light treatment because toxic ROS induced by OG-mediated PDI could attack the cellular wall, proteins, and DNA of microbes. Moreover, the bactericidal effect, as well as the yields of ROS, depended on OG concentrations, irradiation time, and laser output power. Furthermore, we prepared an edible photodynamic antimicrobial membrane comprised of electrospun cyclodextrin nanofibers (NFs) by embedded OG. The resultant OG/HP*β*CD NFs (273.6 μg/mL) under UV-A irradiation for 30 min (14.58 J/cm) could cause a great reduction (>5-Log) of viable bacterial counts of *E. coli*. The situ photodynamic antibacterial activity of OG/HP*β*CD NFs based packaging was evaluated during the Chinese giant salamander storge. Overall, this research highlights the dual functionalities (antibacterial and photodynamic properties) of OG as both an antibacterial agent and photosensitizer and the effectiveness of electrospun NFs containing OG as active antibacterial packaging materials for food preservation upon UV light illumination.

KEYWORDS: *Octyl gallate, photodynamic inactivation, bactericidal mechanism, reactive oxygen species, hydroxyl radical, electrospun nanofibers, foodborne pathogen*

1. INTRODUCTION

The contamination of foodborne pathogens has become a global concern because it is responsible for the deterioration of the organoleptic and nutritional properties of foods during storage and transportation. Driven by the increasing demand of consumers for natural, fresh, nutritious and healthy foods, compared with traditional thermal processes, non-thermal processing technologies are also in high demand. Recently, nonthermal technologies in food processing have gained increased interest and have the potential to replace the traditional well-established food preservation processes, as traditional high-temperature pasteurization could cause undesirable changes in food nutrition, flavor, and texture.[1] Nonthermal technologies such as high hydrostatic pressure, pulsed light, ultrasound, pulsed electric field, cold plasma, and high-pressure homogenization are applied with the purpose of food quality improvement and efficient inactivation of the pathogens.[2] However, these technologies are still struggling with their crucial demerit, including safety concerns toward the food handlers or the high investment cost.[3] Hence, there is an urgent need for a more efficient alternative that processes energy-efficient, safe, reproducible, and cost-effective properties and maintains sufficient antibacterial activity. From this perspective, photosensitization, also known as photodynamic inactivation (PDI), seems to be one of the most promising strategies for non-thermal microbial inactivation in food research with tremendous advantages in food systems including significant inactivation of planktonic cells and eradication of biofilm[4], and effective decontamination of fresh-cut fruits, pieces of beef, pork, and cooked chicken[5].

PDI works when the light of a specific wavelength triggered a series of oxidation reactions inside the cell, and these reactions could occur more easily with the addition of light-sensitive compounds known as photosensitizers (PSs).[6] Moreover, the efficacy of the PDI has been increased by the application of many exogenous PSs such as curcumin, hypericin, chlorophyllin, 5-Aminolevulinic acid, and alpha-terthienyl that interacts with molecular oxygen to produce the reactive oxygen species (ROS) after light excitation, which, in turn, attack cellular components and ultimately destroying the bacterial cells.[7] For instance, the combination of blue light (462 nm) and curcumin exhibited bactericidal activity (>5-Log reduction) against *S. aureus* and *E. coli* compared to blue light or curcumin alone.[8] Our group has been developing various phenolipids with multifunctionalities including antibacterial[9-11] and antioxidant activity, as well as neuroprotective efficacy[12]. In our most recent study, a series of alkyl gallates were prepared using lipase-catalyzed reactions. Among them, octyl gallate (OG) exhibited eloquent antibacterial activity against some related foodborne pathogens.[13] Surprisingly, the potential of OG with low concentration as a novel PS for PDI has been found in this work, which endows OG-mediated PDI with intriguing

bactericidal efficacy to achieve rapid eradication of pathogens and biofilms in a relatively short time due to both photodynamic and intrinsic antibacterial properties of OG itself. Besides, since OG has been permitted for use as an antioxidant additive in food,[14] it is supposed to be safe for humans and can be considered as a promising exogenous PS of PDI. These findings served as a driver of the present study to investigate the potential of OG as an outstanding antimicrobial PS —in the application of PDI for microbiological food safety. Most PDI studies have largely been carried out by using exogenous PS in aqueous solutions,[15] while the poor water-solubility of OG may limit its dispersion in some specific food matrices. Thus, a proper delivery system was needed to develop, such as films or nanofibers made of edible and hydrophilic materials that can uniformly adhere to the foods and deliver OG with photodynamic bactericidal activity.

Since 1934, electrospinning has been recognized as an energy-efficient and simple technology for obtaining continuous micro- or nanofibers.[16] The fibers produced through electrospinning have a thinner diameter and fibrous structure with high porosity and interconnected pores, which make electrospun fibers have been widely used in antimicrobial packaging materials. It is well known that high molecular weight for the polymer with sufficient chain entanglement is one of the essential requirements, in order to obtain nanofibers by electrospinning.[17] However, food packaging materials should not contain any potentially harmful substances for humans. In this context, people have tried to produce biocompatibility and biodegradability nanofibers using non-polymer nature materials, such as cyclodextrin (CD) and tannic acid.[18] Thereinto, CDs are common cyclic oligosaccharides, consisting of (α-1,4)-linked α-L-glucopyranose units with a hydrophilic outer surface and hollow hydrophobic interior and the cone-shaped lipophilic cavity offer a favorable microenvironment for the hydrophobic active substances promoting the formation of inclusion complexes.[19] The high concentration cyclodextrin aqueous solution with sufficient chain entanglement already has been proven to be electrospun into nanofibers successfully. Moreover, the inclusion complexes of CD and active antimicrobial agents were also can be electrospun into nanofibers.[20] The combination of electrospinning and encapsulation provides a useful approach to get the delivery system and enables water-soluble electrospun fibers to be applied in the food industry.

In these scenarios, the salient features of the current study include, (i) investigating the OG-mediated photodynamic bactericidal activity and mechanism against *E. coli*; (ii) developing a novel OG/HP*β*CD nanofibers and further confirming their structures; and (iii) applying the nanofibers containing OG as multi-functionalized food packaging coupled with PDI for the

preservation of Chinese giant salamander. The dual role of OG in improving the production of reactive oxygen species (ROS) as a novel PS on one hand and the enhanced antimicrobial activity as an effective antibacterial on the other, are highlighted for the first time.

2. MATERIAL AND METHOD

2.1. Materials and Light Source

Octyl gallate (OG) was prepared by us and the structure was characterized by ^{1}H NMR and ^{13}C NMR. 2-Hydroxypropyl-*β*-cyclodextrin (HP*β*CD) was purchased from Aladdin and glacial acetic acid (99%, analytical reagent grade) was obtained from Macklin, Shanghai. All other reagents were of analytical grade. A UV-A light chamber was prepared by us and the light source consisted of five UV-A light fluorescent bulbs (18 W, 320-400 nm, peak wavelength 360 nm, Actinic BL, Royal Philips, the Netherlands) mounted on the ceiling of a closed plastic box. The average intensity of UV-A was 8.254±0.18 mW/cm^2, which was measured using an optical power and energy meter (PM100D, Thorlabs, New Jersey, USA) equipped with a silicon power head (S120VC, THORLABS, Newton, USA). For irradiation, the samples were placed at 5 cm from the light source.

2.2. Microbicidal Assay

Escherichia coli ATCC 25922 and *Staphylococcus aureus* ATCC 6538 purchased from the National Center For Medical Culture Collections, Beijing, China were used here. The pre-cultured bacterial cells were inoculated into the fresh Luria-Bertani (LB) medium and grown to an exponential phase at 37 ^{o}C with the agitation of 180 rpm. The strain was used for all experiments to evaluate the efficacy of OG-mediated PDI with UV-A light. The OG+UV-A treatments were performed according to the method[15] with a little modification. The overnight bacterial culture was diluted in sterilized 0.1 and 0.15 mM OG solution prepared in normal saline (NS) to reach a final concentration of approximately 10^6 colony forming units (6 Log CFU/mL) for two bacterial strains. Then, 2 mL of the bacterial suspension was transferred to a well of a 24-well flat-bottom polystyrene plate and followed immediately by UV-A exposure for 15 min. After irradiation, the treated solution was serially diluted in 0.9% (w/v) saline, after which 100 μL of the dilution was seeded on LB agar plates. The plates were incubated at 37 °C for 24 h before enumeration, and the reductions of bacteria were determined. In addition, bacterial suspension incubated in the dark with

OG for the same duration was used as a control.

To examine if the bactericidal effect of OG-mediated PDI could be attributed to ROS, several ROS scavengers CAT (600 U/mL), DMSO (1.0 mM), and TEMPOL(8 mM) were added simultaneously with OG+UV-A treatment. The cultured bacterial with ~6 Log CFU/mL *E. coli* was treated in the absence or presence of UV-A light for 15 min. A group of controls without ROS inhibitor was incubated in the dark for the same time. All samples were subsequently plated and counted via the same method described above.

2.3. Association of OG with *E. coli*

The uptake of OG (or GA) in bacterial cells with or without UV-A irradiation was measured by using diphenylboric acid 2-aminoethyl ester (DPBA).[21] A volume of 1 mL 0.9% (w/v) saline containing approximately 8 Log CFU/mL *E. coli* was mixed with or without GA or OG (0.15 mM) Then, 1 mL of the suspension was transferred into a 24-well plate (Costar 3599, Corning, USA) and exposed to UV-A for 30 min as described previously. After the incubation, each sample was transferred back to the tube and centrifuged at 10,000×g for 2 min to discard the supernatant. The pellet was washed twice using DI water followed by vortexing and then DPBA solution (450 μL, 0.2% w/v in DMSO) was added to the pellet and mixed. In addition, controls were treated in the same manner, but in the absence of phenolics or UV-A irradiation. The final suspension (100 μL)was transferred to a 96-well plate and the fluorescence intensity was recorded with a microplate reader (Multiskan Spectrum 1500, Thermo Electron Corporation, USA) at an excitation/emission wavelength of 405/465 nm. The fluorescence intensity (I) ratio was corrected using the following equation: $[I_{corrected} = I_s - I_o]$, where I_s was the fluorescence intensity reading of the sample with treatments and I_o was the fluorescence intensity of the control.

Quantification of phenolics (OG or GA) adsorption was according to the method reported by Wang et al.[22]. The *E. coli* cells were cultured in LB broth (Hangzhou Microbial Reagent Co. Ltd, China) for 14-16 h. The bacterial cells were harvested and washed three times with PBS (0.1 M, pH=7.2) and then resuspended in PBS to approximately 8 Log CFU/mL. Phenolics were added to the resuspension solution to a final concentration of 0.1 mM. Cells were incubated at 37 °C for 30 min and then harvested. For the quantification of phenolics adsorption, 450 μL of DPBA solution (DMSO, 0.2% w/v) was added to the above bacterial cells and then incubated for 5 min. The images of the cells were captured using confocal laser scanning microscopy (CLSM, Leica TCS SP8, Germany).

182

183 **2.4. Analysis of Reactive Oxygen Species (ROS)**

184 2',7'-dichlorofluorescein diacetate (DCFH-DA) was utilized to assess the generation of ROS in the
185 bacterial cells, was used.[23] The overnight test culture (~8 Log CFU/mL) was treated by OG (0.15
186 mM) with or without ROS scavengers including catalase (CAT), dimethyl sulfoxide (DMSO), or
187 TEMPOL. The CAT, DMSO, and TEMPOL solutions were added into a solution to achieve a final
188 concentration of 600 U/mL, 1.0 mM and 8 mM, respectively. The suspensions were incubated in
189 the dark with OG for the same duration were used as positive controls. After UV-A irradiation for
190 30 min, the excess OG in samples was removed by centrifugation (6000 rpm, 5 min) and the
191 bacteria were resuspended with cold PBS (0.1 mM, pH 7.2-7.4). 10 μM DCFH-DA was mixed with
192 samples and treated in dark at 37 °C for 30 min. The incubated solution was washed twice using
193 PBS. Finally, the fluorescence spectrum of solutions was measured at excitation wavelengths of 484
194 nm with a wavelength of 525 nm with a microplate reader (Multiskan Spectrum 1500, Thermo
195 Electron Corporation, USA). In addition, bacterial suspension with water incubated in dark was
196 used as a negative control, and its fluorescence intensity reading (F_o) was used as the reference to
197 calculate the relative fluorescence unit (RFU) for other treatments using this equation:
198 [Relative fluorescence unit (RFU) $= {F_s}/{F_0}$], where F_s was the fluorescence intensity of the sample
199 with treatments.

200

201 The generation of reactive oxygen species (ROS) in the pathogen cells was visualized using
202 2',7'-dichlorofluorescein diacetate (DCFH-DA) and the CLSM. The overnight test culture (~8 Log
203 CFU/mL) was treated with OG (0.15 mM), UV-A, and OG+UV-A, and suspensions incubated with
204 OG in the dark for the same duration were used as controls. After UV-A irradiation for 30 min, the
205 excess OG in samples was removed by centrifugation (6000 rpm, 5 min) and the bacteria were
206 resuspended with cold PBS (0.1 mM, pH 7.2-7.4). The suspensions with 10 μM DCFH-DA were
207 incubated in dark at 37 °C for 30 min and then centrifugated (6000 rpm) for 5 min. The sample was
208 washed twice with PBS. Finally, the CLSM (Leica TCS SP8, Germany) using ×63 oil immersion
209 objective lens was used to observe the cells, with an excitation wavelength of 484 nm and an
210 emission wavelength of 525 nm.

211

212 Flow cytometry was used to detect intracellular hydroxyl radical formation in *E. coli*.
213 Hydroxyphenyl-fluorescein (HPF) is an anthracene derivative of fluorescein which becomes
214 fluorescent when it was activated by hydroxyl radical.[24] Detailed descriptions of these methods and

analysis are given in SI (Section 1.2).

2.5. Investigation of the Damage of Cell Membranes, proteins and DNA

To evaluate the damage of cell membranes and bacterial proteins, as well as DNA induced by OG+UV-A treatment, the uptake of propidium iodide (PI) (SI, Section 1.3), scanning electron microscope (SEM) (SI, Section 1.4), Sodium dodecyl sulfate-polyacrylamide gel electrophoresis (SDS-PAGE) analysis (SI, Section 1.5) and the agarose gel electrophoresis (SI, Section 1.6) were performed, respectively.

2.6. Electrospinning of Nanofibers (NFs)

The solutions for electrospinning were prepared according to the method described before.[25] The solutions of OG/HP*β*CD inclusion complex (OG/HP*β*CD-IC) were prepared by dissolving HP*β*CD (160%, w/v) in deionized water by 160% (w/v) solid concentration. Then, a proper amount of OG (OG: HP*β*CD=1:1 and 1:2, mol/mol molar ratio) was added into aqueous CD solutions and the mixtures were stirred at room temperature for 12 h to obtain clear and homogeneous OG/HP*β*CD-IC solutions for electrospinning. The pure HP*β*CD solution (160%, w/v) was also prepared as blank control. A physical mixture of HP*β*CD and OG (OG/HP*β*CD PM) was obtained by grinding in a mortar (OG: HP*β*CD =1:1, mol/mol).

The prepared OG/HP*β*CD-IC solutions were placed into a 10 mL plastic syringe fitted with a 23G (outer/inner diameter; 0.64 mm/0.33 mm) metal needle. The loaded syringe was fixed horizontally with a syringe pump (Baoding longer, LSP03-1A), the flow rate was adjusted to 1 mL/h. The electrode of the high voltage power supply (Tianjin Dongwen, DWLP303-1ACDB) was connected to the metal needle tip and the nanofibers were received on an aluminum foil sheet which was covered on a grounded metal collector at a distance of 15 cm from the needle. By varying the collection time, the mass of the fibers per surface area can be adjusted. The electrospinning process was performed under ambient temperature and the relative humidity of 25 ^{o}C and 45%, respectively. The collected fibers were vacuum dried for 24 h to remove solvent residue.

2.7. Characterization of HP*β*CD/OG-IC Nanofibers

Proton NMR (^{1}H-NMR) spectra were recorded by the NMR spectrometer (Bruker AMX-300) at 25

°C. ^{1}H-NMR was utilized to calculate the molar ratio between OG and HP*β*CD in OG/HP*β*CD-IC nanofibers. Pure OG and OG/HP*β*CD-IC nanofibers were dissolved in DMSO-d6 at 40 g/L sample concentration using tetramethylsilane (TMS) as the internal standard. The integration of chemical shifts (δ, ppm) and the discrete peaks of samples were analyzed and calculated by Mestranova software. Fourier-transforms infrared spectroscopy (FTIR) OG, HP*β*CD, OG/HP*β*CD nanofibers, and OG/HP*β*CD PM were recorded in the wavenumber range of 400-4000 cm^{-1} on a Nicolet 380 instrument (Thermo Nicolet Ltd., USA). The crystal structure of samples was analyzed by X-ray diffraction (XRD)[26] on a D8 Advance X-ray diffractometer equipped with a copper tube, and an X-ray source was operated at 45 kV and 35 mA. The diffraction pattern was obtained at room temperature (25 °C), the 2*θ* angle was set from 3° to 50° with a scan rate and scanning speed of 0.02 ° $min^{-1}$and 4 ° min^{-1}, respectively. Differential scanning calorimetry (DSC) (TA Q2000, USA) was used for the study of the thermal properties of the samples. The nanofibers (5 mg) were equilibrated at 25 °C and then heated to 250 °C at a heating rate of 10 °C min^{-1} under the nitrogen atmosphere. The surface morphology of nanofibers was recorded using SEM (Hitachi T-1000, Hitachi High-Technologies Corporation, Tokyo, Japan). The fibers were set on a metallic stub and covered with gold under a vacuum in an argon atmosphere. The coated samples were viewed in the SEM operating at an acceleration voltage of 15 kV. The average fiber diameter (AFD) of nanofibrous was measured and analyzed using Image software with 100 fibers from each SEM image.

2.8. Bacterial Photoinactivation Studies of OG/HP*β*CD NFs

The photodynamic antimicrobial activity of OG/HP*β*CD NFs was assessed against *E. coli*. The overnight bacterial culture was diluted in sterile 0.9% w/v saline to reach a final concentration of approximately 6 Log CFU/mL, and a proper amount of OG/HP*β*CD nanofibers was added into the suspension to reach a final concentration of 182.4 and 273.6 μg/mL. Then, the cell suspension of 2 mL was added to one well of a 24-well flat-bottom polystyrene plate and followed immediately with light exposure of 30 min. In addition, the cell suspension incubated in the dark with OG/HP*β*CD nanofibers for the same duration was used as a control. All samples were subsequently plated and counted using the method mentioned in 2.2.

2.9. Effects of Photodynamic inactivation of OG/HP*β*CD NFs on Chinese Giant Salamander Preservation

To assess the antimicrobial activity of OG/HP*β*CD-IC NFs, a Chinese giant salamander

preservation test was performed. The salamander meat cubes (3 cm×3 cm×1 cm, 10 g) were cut under aseptic conditions, then, one side of each meat cube was inoculated by immersion in a bacterial suspension of *E. coli* (4 Log CFU/mL) for 30 seconds. The treated salamander meats were singly sealed with OG/HPβCD NFs and followed immediately by UV-A irradiation for 5 min at a distance of 5 cm. Samples covered with nothing were used as controls. After selected treatments, samples were mixed with 40 mL PBS (0.1 M, pH 7.2) and beat for 2 min with a slap homogenizer to collect the bacteria from the surface of salamander meat. 1 mL of the solution was serially diluted and spread on LB agar plates for CFU counting. To further investigate the effect of OG/HPβCD NFs on the preservation of Chinese giant salamander, the changes in the total viable count and flavor of samples during the storage of samples were studied. Briefly, after the samples were treated with the methods described above, they were singly packed and sealed in polystyrene film and stored at 4 ^{o}C for 15 days. The number of colonies on the surface of the salamander was counted every 3 days to evaluate the antibacterial activity of nanofibers. According to the methods of Shi et al.[13], the flavor analysis using an electronic nose was also performed on salamander from batches control, control+UV-A, OG/HPβCD NFs and OG/HPβCD NFs+UV-A at 4 ^{o}C for 15 days (for more details was given in SI (Section 1.8) and Figure S1). Five repetitions were performed for each group.

2.10. Statistical Analysis

Results were expressed as the mean ± standard deviation. Statistical significance between different treatments was determined using t-test; *P*-values $\leq$0.05 were used to determine significant differences.

3. RESULTS AND DISCUSSION

3.1. Bactericidal Effect of the OG-mediated PDI against *E. coli*

We evaluated the use of UV-A light irradiation in combination with octyl gallate (OG) as an alternative approach to achieve *E. coli* inactivation and the results are summarized in Figure 1. In Figure 1A, viable bacterial counts of *E. coli* without any treatment were ~6.80 Log CFU/mL, and no significant change was observed in the sample only treated with UV-A light for 30 min (14.85 J/cm^2). When *E. coli* was treated with different concentrations of OG for 30 min, it was killed to a

degree depending on the concentration of OG regardless of the usage of UV-A irradiation. However, the UV-A irradiation significantly reduced (P<0.01) the bacterial count for all samples treated by OG, compared to the corresponding samples without UV-A irradiation. Generally, the viable count of bacteria is reduced in an OG-concentration dependent manner. Without UV-A irradiation, *E. coli* cells were decreased from 6.2 Log CFU/mL to 4.3 Log CFU/mL (P<0.05) as the OG concentration increased from 0.05 mM to 0.15 mM. However, under 14.85 J/cm^2 irradiation of UV-A, the *E. coli* cells were decreased from 4.8 Log CFU/mL to 4.0 Log CFU/mL when the OG concentration was elevated from 0.05 mM to 0.1 mM. Moreover, none of the bacterial cells could be detectable when treated by 14.85 J/cm^2 irradiation with 0.15 mM OG within 30 min.

In Figure 1B, compared to the positive controls with only UV-A irradiation, significant decreases (P<0.01) of bacterial cells were observed in all samples with the OG-mediated PDI. Also, the UV-A irradiation time (dosage) significantly affected the activity of *E. coli.* After 15 min UV-A irradiation with OG (0.05, 0.1, and 0.15 mM), the *E. coli* cells were decreased to 5.4, 4.4, and 2 Log CFU/mL (P<0.01), respectively. However, an obvious and continuous reduction in the bacterial cells was observed when UV-A irradiation time was extended from 15 min to 30 min. Thus, the OG-mediated PDI against *E. coli* was typically dependent on the photosensitizer concentration- and irradiation dosage.

As shown in Figure 1C, as for either *E. coli* or *S. aureus*, when the bacteria suspension containing OG was exposed to UV-A light at 365 nm and an irradiance of 8.254±0.18 mW/cm^2, viable counts decreased in a time-dependent manner. Compared with other treatments, the combination of 0.15 mM OG and UV-A light exhibited the greatest bactericidal activity, achieving >4.5-Log CFU/mL reduction of *E. coli* within 15 min and >6-Log CFU/mL reduction of *S.aureus* within only 5 min. Although treatment only with the UV-A irradiation performed in this present study was not effective (<1-Log CFU/mL), OG+UV-A irradiation treatment could noticeably kill the bacteria, indicating that the tremendous increase in the bactericidal effect was not solely due to the OG alone treatment or UV-A light exposure. The combination of OG and UV-A illumination has a stronger synergistic effect on both *E. coli* and *S. aureus* in vitro. Although a synergistic interaction between 10 mM gallic acid (GA) and UV-A (365 nm) light to inactivate *E. coli* O157:H7 had been also reported,[27] OG was used in this present study at a concentration of less than one-sixtieth of it (0.15 mM), indicating that photodynamic bactericidal effect of OG on bacterial cells is superior to that of GA. Also, the effect of propyl gallate (PG, 10 mM)+UV-A on the inhibition of *E. coli* O157:H7 was lightly stronger than that treated by GA (10 mM)+UV-A.[22] Furthermore, Gram-positive

bacteria, *S. aureus*, tended to show higher susceptibility to either 0.15 mM OG alone or the OG+UV-A light treatment than Gram-negative bacteria, *E. coli*, which may be related to differences in the cellular membranes.[10] On the other hand, Nakamura et al.[28] reported that the exposure of LED light (400 nm; 260 mW/cm^2) in the presence of 5.88 mM GA within the suspension of *E. coli* caused more than 5-Log CFU/mL microbial reduction. By contrast, in the present study, neither 0.15 mM GA alone nor the combined treatment with UV-A irradiation showed substantial bactericidal properties (<1-Log CFU/mL). It is worth noting that, under the dark condition, OG showed rather higher bactericidal activity than GA (Figure 1C). Although the bactericidal activity of GA was also observed, OG exerted stronger bactericidal capacity than GA because *S. aureus* and *E. coli* were effectively killed by OG alone in LB media, at very low concentration, presenting an MBC of 0.1 mM and0.2 mM for *S. aureus* and *E. coli*, respectively (Table S1).

The acquired results suggested that (1) the antimicrobial potency of OG depends largely on the hydrophobic portion (the alkyl group) of the molecule, which could offer more affinity to the bacterial membranes. It is also in accordance with the findings from Kubo et al.[29] and us[13]. (2) As for the OG-mediated PDI, the OG alone or UV-A light irradiation was not solely responsible for the remarkable microbial reduction, which further corroborates the occurrence of interaction between OG and UV-A light. OG is very promising as an "antibacterial photosensitizer" with outstanding antibacterial as well as photodynamic activity.

[Figure 1]

3.2. Cellular Uptake of OG in *E. coli*

To gain further insight into the mechanisms underlying the antibacterial effects of OG-based PDI, we firstly analyzed the binding affinity of OG toward bacteria. In the present case, DPBA was employed to detect the cellular uptake of either OG or GA in *E. coli* because it becomes fluorescent when it combines with flavonoid compounds.[21] Figure 2A shows that *E. coli* treated with OG+UV-A has a higher fluorescent intensity (286.37 ± 8.92) than that incubated with OG alone (153.03 ± 13.3), indicating that the exposure of UV-A increased the level of OG uptake in cells. The uptake of GA by bacteria was similarly affected by the UV-A irradiation. However, the extent of uptake of OG is significantly higher (P<0.05) than that of GA regardless of the absence or presence of UV-A irradiation, further indicating OG showed a higher affinity to bacteria than GA. One of the

possible factors responsible for the discrepancy in the affinity to bacteria between OG and GA might be due to the difference in their hydrophobicity. As shown in Table S1, the Log *P* value of OG is 4.63 while the Log *P* value for GA is 0.4. Both of them possess the same hydrophilic portion, a pyrogallol group, thus distinguishing the role of the hydrophobic alkyl portion of OG, as discussed in our previous studies.[10,11,12] Moreover, the variation trend of the OG uptake was consistent with the photodynamic inactivation results in Figure 1C, indicating that the cellular uptake of OG was a vital factor for OG-mediated PDI and the higher uptake of OG under UV-A light exposure enhanced the bactericidal effect.

To further verify the association or affinity of OG or GA to bacteria, the cellular internalization of them at 0.1 mM was studied by using a confocal microscopy. As observed in Figure 2B, OG treated groups showed stronger fluorescence intensity than GA treated groups, suggesting that the intracellular uptake of OG was higher than that of GA. Moreover, compared to the low level of internalization GA, significant amounts of OG were acquired in *E. coli* as early as 15 min. These results further illustrated that OG could become a very promising alternative photosensitizer for PDI to induce a more effective photokilling of pathogenic microbial cells than GA because the amphiphilic property of OG effectively triggers its fast cellular uptake, leading to the increased intracellular uptake.

[Figure 2]

3.3. Antimicrobial Effects of OG-mediated PDI via Multiple Mechanisms of Action

OG and UV-A Induced ROS Generation

It had been reported that ROS generation, especially interior hydroxyl radicals (•OH), is a critical aspect in the antibacterial activity of photoirradiated polyphenols against a broad range of pathogens.[28] As such, we further examined if the generation of ROS in *E. coli* could be one of the mechanisms for the bactericidal activity of the OG-based PDI with UV-A irradiation. Thus, a fluorescent probe, DCFH-DA, was used for measuring intracellular oxidative stress in cells. In Figure 3A, bacteria exposed to UV-A light exhibited significantly higher fluorescence intensity than the corresponding samples in the dark. Moreover, *E. coli* treated with OG+UV-A light had the highest fluorescent intensity, followed by the treatment with OG alone, representing the efficient intracellular ROS production during the OG-mediated PDI. On the other hand, it is noteworthy that *E. coli* treated by 0.15 mM OG alone for 30 min also had significantly higher fluorescence intensity

than samples treated by 0.15 mM GA alone, which was consistent with their antibacterial results in Figure 1C. Additionally, it also indicated that ROS production induced by OG itself could be essential for OG-induced killing in the dark, which is in agreement with our previous report that the internalized OG may interfere with the activity of ETC on the cytoplasmic membrane of *E. coli*, promoting the generation of toxic ROS and leading to consequently bacterial death.[13] Furthermore, the ROS was visualized by confocal laser scanning microscopy (Figure 3B). Briefly, the combination of OG with UV-A irradiation led to a higher level of intracellular ROS generation, suggesting that UV-A light irradiation played a pivotal role in the production of ROS during the OG-mediated PDI.

Several radical scavengers, including H_2O_2 scavenger (CAT), •OH scavenger (DMSO), and $•O_2^-$ scavenger (TEMPOL) were utilized to further confirm which type of ROS was mainly involved in OG-mediated PDI. As shown in Figure 3C, compared with the samples incubated with OG alone, significant reductions in the fluorescence intensity with the addition of these scavengers were observed under the same treatments. More specifically, either CAT or DMSO showed better efficacy in inhibiting the production of ROS, as compared to TEMPOL. Especially, this discrepancy was more pronounced in UV-A irradiated samples. Besides, the relationship between the generation of ROS and bactericidal activity was also examined. As expected, the concentration of ROS produced in bacteria was accordant with the inhibitory effect of the treatment. To be more precise, the addition of CAT and DMSO could lead to a larger increase in bacterial survival than in the presence of TEMPOL and this effect was more clear in the presence of UV-A light (Figure 3D). The attenuation of the antibacterial effect of OG+UV-A by these radicals scavengers further supports the assumption that ROS was conspicuously responsible for the bactericidal activity. These findings indicated that the OG and UV-A interaction effectively promoted the production of ROS, which is essential for the bactericidal activity of OG-mediated PDI. Moreover, the ROS mainly involved in OG-mediated PDI were probably, H_2O_2 and •OH. Arakawa et al.[30] reported that H_2O_2 synthesis by (−)-epicatechin gallate is attributed to its bactericidal activity, which was enhanced with higher pH conditions (>pH 6). Other researchers also found that catechins and other polyphenolic compounds could cause H_2O_2 generation in solutions under neutral or alkaline conditions.[31,32] In this study, OG was dissolved in PBS (0.1 M, pH 7.2-7.4). Thus, as for the ROS generation, it was rationalized that the autoxidation of OG should be considered and a possible mechanism related to the autooxidation of OG catalyzed by UV-A in aqueous solutions could be proposed in Scheme 1. Using UV-A as the oxidizing source, OG can be oxidized to quinone or hydroxyl related derivatives with the formation of H_2O_2 in the presence of dissolved oxygen, owing

to the tendency of the three aromatic hydroxyl groups of OG to undergo autooxidation or oxidation.[33] In this case, H_2O_2 would be photolyzed by UV-A irradiation to form •HO radicals.[35] UV-A irradiation of 0.15 mM OG generated the highest level of ROS, indicating that 365 nm light can significantly promote OG autooxidation. On the other hand, the internalized OG may interfere with the activity of ETC on the cell membranes of *E. coli*, also producing toxic ROS.[13] As the oxidative power of each ROS is taken into account, the reactivity and the oxidative power of •OH are much than those of H_2O_2 or $•O_2^-$[36]. In addition, 500 mM H_2O_2 can kill *S. aurous* only with 1-Log reduction[37]. Together, it is reasonable to assume that H_2O_2 would probably act as a source of •OH in the photolysis reaction, rather than be a major contributor to the bactericidal action in a short time (15-30 min) [13], which is in agreement with the results reported by Nakamura et al.[36]

The intracellular •OH formation in the bactericidal action of OG-mediated PDI was also substantially confirmed by the flow cytometry with the dye HPF.[38] The histogram distribution in Figure 4E showed the contents of intracellular •OH radicals of different groups. There is a significant increase in fluorescence intensity when *E. coli* was exposed to OG+UV-A. In sharp contrast, single UV-A exposure stimulates no hydroxyl radical production, and a lower hydroxyl radical content was observed when the bacteria were treated with OG only. Moreover, we found DMSO significantly reduced •OH formation induced by the duo. These findings substantially confirmed the existence of •OH radicals bactericidal pathway directly associated with OG+UV-A induced bacterial death.

[Figure 3]

OG and UV-A Induced Alterations in Bacterial Cell Membrane, proteins and DNA

Since OG has a high affinity to the cell membrane, it can facilely permeate into the outer membrane and further damage the cell membrane. It had been observed to disintegrate bacterial outer membrane by some researchers[39] and us[10, 11]. On the other hand, OG internalized immediately by the cells would trigger oxidative stress in bacteria. Consequently, the •OH generated around the phospholipid membrane of the bacteria will further compromise the cell membranes. Similar to UV light and some other phenolic compounds[27,33], UV light together with OG damaged cell envelopes yet in a greater efficacy (P<0.05) than either alone as assessed by propidium iodide (PI) staining[40] (Figure 4A). Moreover, the synergistic effect of photolytic OG caused remarkable microbial inactivation (>5-Log) within 30 min and *S. aureus* within only 5 min (Figure 1C) and the dramatic cellular alterations were ultrastructurally corroborated with SEM showing irreversibly devastated

cell envelopes (Figure 4B-c). In sharp contrast, only shrinkage and irregular shape of the surface (Figure 4B-b) for cells treated by OG alone could be observed compared to the control (Figure 4B-a), indicating that the mechanism of bactericidal activity caused by 0.15 mM OG alone has less to do with the damage of membrane, but more to do with the ROS triggered by OG. It is also consistent with the findings by Kuto et al. [41] and Wang et al.[22] Furthermore, it is worth to be noted that the tendency in PI uptake (Figure 4A) is also in consistency with the findings of cellular uptake in Figure 2A, indicating cellular uptake of phenolics correlated positively with the damage of the bacterial membrane. As for the samples treated with GA or NS, although the fluorescence intensity of bacteria treated by GA+UV-A or UV-A light alone (NS) was significantly higher than their correspondings (Figure 4A), no bactericidal effect could be observed and logarithmic reduction of CFU/mL in these cases was <1-Log (Figure 1C).

SEM was used to further observe alternations in the surface morphology of *E. coli* treated by OG-mediated PDI. Samples treated by 0.15 mM OG without UV-A exposure exhibit uneven and slightly shriveled appearance (Figure 4B-b), with a comparison of regular rod shape of controls (Figure 4B-a). However, with simultaneous UV-A and OG treatment for 30 min, *E. coli* cells were damaged severely, with a lot of debris (Figure 4B-c), indicating that membrane damage was strongly correlated with the bactericidal effect of OG-mediated PDI.

The mentioned ROS may induce oxidative damage to bacterial proteins and DNA and ultimately lead to bacterial death.[42] The alterations of membrane proteins of *E. coli* upon OG-mediated PDI were evaluated by using SDS-PAGE. Figure 4C showed that 14.85 J/cm^2 UV-A irradiation alone causes no effects on the membrane protein integrity of *E. coli*. Only OG at 0.15 mM caused a slight reduction in the band intensity. In contrast, OG+UV-A irradiation caused a significant decrease of band intensity, especially for ~29 kDa, 40 kDa, and ~60 kDa protein. These results highly suggested that the synergism effect between OG and UV-A irradiation on the damage of membrane proteins of *E. coli* is stronger than that of the individual in the equivalent dose and OG as an exogenous photosensitizer might play a role in killing *E. coli* in comparison with the UV-A irradiation. The FTIR spectra revealed differences in peak appearance, as well as the relative intensity of the membrane protein with different treatments. The ratio of amide I (1640 cm^{-1}) to amide II (1510 cm^{-1}) bands predominantly associated with proteins varied with the OG+UV-A treatment (Figure 4E). The intensity of amide I and amide II was higher when cells were incubated with OG under UV-A exposure, illustrating the variability in membrane proteins of *E. coli* with different structural and functional integrity related to these treatments. On the other hand, if photo-oxidation of OG is

the same way proposed in Scheme 1, a postulated main chemical pathway involves oxidization of OG, generating quinone intermediates that could react with nucleophiles (mainly amino or sulfhydryl side chains of membrane proteins) to form covalent C-N or C-S bonds with the phenolic ring (cross-linking chemistry), leading to the further damage of the bacteria.[43] However, the more possible involvements of quinones with bacterial proteins should be further studied by us in the future.

The genomic DNA is also the main target of ROS. As such, except for the damage to the cell membrane and protein, the effect of OG-based PDI on the damage of the genomic DNA of *E. coli* is measured and shown in Figure 4E. the treatment by UV-A irradiation alone cause no significant changes in the band intensity of genomic DNA compared to the control, indicating individual UV-A irradiation didn't display sufficient damage towards the genomic DNA of *E. coli*. The band intensity of the group treated with OG or OG+UV-A was significantly decreased and the treatment of OG+UV-A almost completely wreck the integrity of the genomic DNA of *E. coli*, which is also consistent with both the generation of ROS in Figure 3 and the bactericidal results in Figure 1. These discrepancies of damage towards the genomic DNA could be reasonably explained by the difference in the generation of intracellular ROS induced by 0.15 mM OG alone and OG+UV-A. These results are also consistent with the previous study of curcumin-medicated PDI on the genomic DNA of *L. monocytogenes*.[44]

[Figure 4]

3.4. Proposed Multi-mechanism of OG-mediated PDI

A possible scheme for the bactericidal action of OG-mediated PDI is illustrated in Scheme 1. On the one hand, OG by itself exerts an antimicrobial ability through interacting with the bacteria cell membrane because its hydrophobic portion offers it a high affinity to the membrane. Then, OG can induce membrane rupture and the release of cell components. Besides, while OG with polyphenolic hydroxyl groups would be photo-oxidized by the UV light peaked at 365 nm into quinone or semiquinone derivatives, a proton-coupled electron transfer to dissolved oxygen would result in generating H_2O_2. Then the photolysis of H_2O_2 would be catalyzed by the UV light to produce more reactive•OH radicals. Also, internalized OG can interfere with the activity of the electron transport chain (ETC) on the cytoplasmic membrane, resulting in excessive production of toxic ROS including •OH[13]. Consequently, •OH from two such possible pathways would cause severe oxidative damages to biomolecules such as lipid, protein and DNA. On the other hand, Quinone

intermediates generated from a postulated main chemical pathway involving oxidization of OG could react with amino or sulfhydryl side chains of membrane proteins through the cross-linking chemistry, leading to further damage to the bacteria. Therefore, the chances that microbes can develop tolerance or resistance to OG-mediated PDI must be considered highly unlikely because the development of antimicrobial resistance is not supposed to occur due to multimodal mechanisms of antibacterial action.[45]

[Scheme 1.]

3.5. Characterization of Electrospun Fibers

Figure S2 displays the phase solubility profiles of OG/HP*β*CD-ICs, showing the A-type profile.[46] The apparent stability contents (K_c) of *β*CD/OG-IC were calculated as 5436 M^{-1} (R^2>0.99), indicating the existence of an extremely strong interaction between OG and HP*β*CD cavity. Then, the parameters of the electrospinning process were optimized to get bead-free and uniform nanofibers using OG/HP*β*CD-IC solution. Figure 5A shows the SEM images of the nanofibrous films and their average fiber diameter (AFD) distribution. The pure HP*β*CD NFs displayed fibers with a few beads. In sharp contrast, the OG/HP*β*CD NFs without any beaded morphology were successfully achieved and its mats exhibited self-standing, lightweight, and flexible characteristics. The AFD of pure HP*β*CD NFs and OG/HP*β*CD NFs (1:1) were 981.6±504.3 nm and 452.6±221.24 nm, respectively. Solutions with proper conductivity and viscosity have sufficient aggregation and interactions between molecules which ensure the formation of uniform nanofibers.[47] Typically, the solution with lower viscosity and higher conductivity has much more stretching and leads to the formation of thinner fibers. Pure HP*β*CD NFs with a few beads were mostly formed by using HP*β*CD solutions having low conductivity. It may be unfavorable for the full stretching of the electrospinning jet. The addition of OG to the HP*β*CD solution resulted in a decrease in viscosity and an increase in the conductivity of the solution. Compared to HP*β*CD solutions, the viscosity of OG/HP*β*CD (1:1) solutions was decreased from 1.97±0.05 Pa s to 0.97±0.02 Pa s, and its conductivity was increased from 15.61 μS/cm to 28.01 μS/cm (Table S2). Hence, the OG/HP*β*CD NFs have an average AFD value of 452.6±221.24 nm which was smaller than that of pure HP*β*CD NFs.

^{1}H NMR can be used to detect the interaction of hydrogen bonds in a molecule and the surrounding chemical environment to prove the presence of OG and calculate the molar ratio of OG/HP*β*CD NFs. For OG/HP*β*CD NFs, the ratio of OG/HP*β*CD was confirmed according to the -CH_3 protons of

HPβCD at 1.03 ppm and aromatic protons of OG at 6.9 ppm (Figure 5B). The results indicated that for the OG/HPβCD NFs, the OG was encapsulated completely. It is consistent with the previous study related to the HPβCD/Ibuprofen nanofibers[25]. FTIR analyses for OG/HPβCD NFs were performed to affirm the inclusion complexation between OG and CD molecules. Figure 5C presents the FTIR spectra of HPβCD NFs, OG, and OG/HPβCD NFs. A discernible stretching peak from 3000 and 3600 cm^{-1} is the -OH group in HPβCD.[20] However, in the FTIR spectra of OG/HPβCD NFs, the characteristic bands located 3347 cm^{-1} and 3450 cm^{-1} of OG were disappeared, and the bands located at 1608 cm^{-1}, 1667 cm^{-1}, 2852 cm^{-1} and 2916 cm^{-1} were shifted to higher frequencies with reductions in intensity. These results revealed the changes of characteristic bands of the pure components and proved the formation of OG/HPβCD-IC. The crystalline structure of OG/HPβCD NFs was confirmed using XRD analysis. As shown in Figure 5D, OG presents one sharp and intense characteristic diffraction peaks at 4.2° and other peaks located at 12.8°, 13.9°, 15.4°, 19.8°, 20.8° 21.5°, and 26.5°, reflecting its crystalline nature. The diffraction pattern of HPβCD exhibits two broad halos at 10.2° and 18.6°, showing its amorphous nature which was retained after the formation of HPβCD/OG NFs. XRD graphs show that HPβCD/OG NFs have amorphous characteristics without showing any specific OG diffraction peak, strongly suggesting the formation of the inclusion complex between CD and OG. The formation of OG crystals is not supposed to occur because OG is encapsulated into the CD cavity prevents, resulting in separating OG molecules from each other. A similar result that new peaks appeared at 6.9°, 13.1° and 19.7° in the diffraction pattern of HPβCD/Ibuprofen-IC nanofibers was also obtained before[25]. DSC is also employed to confirm whether OG is encapsulated in the CD cavities or not. In Figure 5E, the pure OG thermogram showed an obvious endothermic peak at near 100 °C, which corresponded to its melting point. Conversely, there is no endothermic peak at this point for OG/HPβCD NFs, revealing that OG was fully encapsulated by HPβCD. These findings were consistent with the results that the displacement of the endothermic peaks at 167.19 °C and the reduction of intensity in the DSC curves of GA and HPβCD encapsulation in comparison with that of pure substances, indicating the formation of the inclusion complex of GA and HPβCD.[48]

[Figure 5]

3.6. Studies of Bacterial Photoinactivation of OG/HPβCD NFs

Following the successful preparation of OG/HPβCD NFs, we next investigated its antibacterial photodynamic activity against *E. coli*. As observed in Figure 6A, the combination of OG/HPβCD NFs and UV-A exposure could lead to remarkable reductions in bacterial counts. When the final

concentration of OG/HP*β*CD NFs was 273.6 μg/mL under UV-A irradiation for 30 min (14.58 J/cm), there was a great reduction (>5-Log) of viable bacterial counts (Figure 6A-a). Also, the photodynamic antibacterial efficacy of OG/HP*β*CD NFs increased with increasing the sample concentration and the dosage of UV irradiation (Figure 6A-b). On the other hand, only UV-A exposure treatment exerted little bactericidal effect against test strains. Compared to the control, 273.6 μg/mL OG/HP*β*CD NFs alone could also exhibit antibacterial activity to *E. coli*, as the incorporation of OG into the electrospun NFs still can maintain its antibacterial activity. These data also confirmed the feasibility of OG/HP*β*CD NFs to release OG in a physiological medium to photodynamically inactivate *E. coli*.

3.7. Effect of a Combination of OG/HP*β*CD-IC NFs Based Packaging and PDI on Chinese Giant Salamander Preservation

The situ antibacterial activity of OG/HP*β*CD NFs based packaging was evaluated during the storge of Chinese giant salamander. The contaminated salamander meat was packed with OG/HP*β*CD NFs in the dark or under UV-A exposure. Figure 6B showed the results of OG/HP*β*CD NFs combined with PDI against *E. coli* on the surface of salamander. The bacterial count was reduced by ~57% and ~99% in 5 min treatment, respectively, suggesting that OG/HP*β*CD NFs are of potential value as either antibacterial agents or photosensitizers carrier to inactivate the *E. coli* with UV-A irradiation, and improve the safety and shelf life of fresh perishable food during storage. Figure 6C reports the total viable count (TVC) of salamander meat after selected treatments during the storage. Samples packed with OG/HP*β*CD NFs with or without UV-A irradiation have a lower initial bacterial count as described above, and the number of colonies maintained at a low level (<3 Log CFU/g) during the storage, especially for the group treated with UV-A irradiation. Conversely, the TVC of control rose rapidly to 7.5 Log CFU/g after 15 days of storage. These findings further confirm that OG plays a dual role as an antibacterial agent and photosensitizer of PDI to effectively mitigate foodborne pathogens. Moreover, as food will produce a large amount of different volatile gases during storage, the electronic nose (ENS) can be utilized to discriminate the gas and then judge the freshness of the food. The smell of stored salamander meat was clearly distinguished from the fresh reference by ENS after 15 days of storage (Figure 6D). The PCA region of salamander meat packaged with OG/HP*β*CD NFs combined with UV-A irradiation was the closest to the fresh reference than other samples, indicating that this combined treatment can effectively maintain the quality of salamander meat. These results indicated that OG/HPβCD NFs as active food packaging materials can prevent the contamination of foodborne pathogens, consequently, ensure the quality

and safety of fresh perishable food.

[Figure 6]

The present study demonstrated that OG-mediated PDI could exert rapid and superior bactericidal activity against foodborne bacteria. The dual role of OG as a promising photosensitizer as well as an antibacterial agent has been highlighted for the first time. We also elaborated the multi-mechanism of synergistic bactericidal action by simultaneous OG+UV-A treatment that might be related to oxidative stress and the covalent interaction between quinones and bacterial proteins through the cross-linking chemistry. Furthermore, the electrospun cyclodextrin nanofibers incorporated with OG were fabricated with excellent photodynamic antibacterial activity under UV-A irradiation and also effectively reduced bacteria on the surface of the Chinese giant salamander. Therefore, the efficient and photodynamic antibacterial activity of edible OG encapsulated electrospun cyclodextrin nanofibers demonstrate the vast potential to become novel multifunctional food packaging materials in food sterilization and fresh-keeping processing.

ABBREVIATION

Octyl gallate, OG
Gallate acid, GA
Photodynamic inactivation, PDI
Photosensitizers, PSs
Reactive oxygen species, ROS
Hydrogen peroxide, H_2O_2
Hydroxyl radicals, •OH
Superoxide anion, $•O_2^-$
Electron transport chain, ETC
Propidium iodide, PI
Diphenylboric acid 2-aminoethyl ester, DPBA
4-hydroxy-2,2,6,6-tetramethylpiperidine-1-oxyl; TEMPOL
2-Hydroxypropyl-*β*-cyclodextrin, HP*β*CD
Fourier transform infrared, FTIR
X-ray diffraction, XRD
Differential scanning calorimetry, DSC
Total viable count, TVC

674 Electronic nose, ENS
675 *Escherichia coli*, *E. coli*
676 *Staphylococcus aureus, S. aureus*
677

678 **ACKNOWLEDGEMENTS**

679 The work was supported by the National Natural Science Foundation of China (21106131),
680 Zhejiang Province Public Welfare Technology Application Research Project (LGJ19C200001),
681 Academic Exchanges and Talent Training Program (2017SICR109), Zhejiang Provincial Program
682 for Overseas High-Level Experts Introduction (Z20170407), as well as Food Science and
683 Engineering the Most Important Discipline of Zhejiang Province (JYTsp20142101).
684

685 **REFERENCES**

686 [1] Van Impe, J.; Smet, C.; Tiwari, B.; Greiner, R.; Ojha, S.; Stulić, V.; Vukušić, T.; Režek Jambrak,
687 A. State of the Art of Nonthermal and Thermal Processing for Inactivation of
688 Micro-Organisms. *J. Appl. Microbiol.* **2018**, *125*, 16-35.
689 [2] Ortega-Rivas, E.; Salmerón-Ochoa, I. Nonthermal Food Processing Alternatives and Their
690 Effects on Taste and Flavor Compounds of Beverages. *Crit. Rev. Food Sci. Nutr.* **2014**, *54*,
691 190-207.
692 [3] Josewin, S. W.; Ghate, V.; Kim, M. J.; Yuk, H. G. Antibacterial Effect of 460 nm
693 Light-Emitting Diode in Combination with Riboflavin against *Listeria Monocytogenes* on
694 Smoked Salmon. *Food Control.* **2018**, *84*, 354-361.
695 [4] Chen, B.; Huang, J.; Li, H.; Zeng, Q. H.; Wang, J. J.; Liu, H.; Pan, Y.; Zhao, Y. Eradication of
696 planktonic *Vibrio parahaemolyticus* and its sessile biofilm by curcumin-mediated
697 photodynamic inactivation. *Food Control*. **2020**, *113*, 107181.
698 [5] Corrêa, T. Q.; Blanco, K. C.; Garcia, É. B.; Perez, S. M. L.; Chianfrone, D. J.; Morais, V. S.;
699 Bagnato, V. S. Effects of ultraviolet light and curcumin-mediated photodynamic inactivation
700 on microbiological food safety: A study in meat and fruit. *Photodiagn. Photodyn.* **2020**, *30*,
701 101678.
702 [6] Ghate, V. S.; Zhou, W.; Yuk, H. G. Perspectives and Trends in the Application of
703 Photodynamic Inactivation for Microbiological Food Safety. *Compr. Rev. Food Sci. Food Saf.*
704 **2019**, *18*, 402-424.

[7] Luksiene, Z.; Zukauskas, A. Prospects of Photosensitization in Control of Pathogenic and Harmful Micro-Organisms. *J. Appl. Microbiol.* **2009**, *107*, 1415-1424.

[8] Bhavya, M. L.; Umesh Hebbar, H. Efficacy of Blue LED in Microbial Inactivation: Effect of Photosensitization and Process Parameters. *Int. J. Food Microbiol.* **2019**, *290*, 296-304.

[9] Shi, Y.; Wu, Y.; Lu, X.; Ren, Y.; Wang, Q.; Zhu, C.; Yu, D.; Wang, H. Lipase-catalyzed esterification of ferulic acid with lauryl alcohol in ionic liquids and antibacterial properties in vitro against three food-related bacteria. *Food Chem.* **2017**, *220*, 249-256.

[10] Shi, Y.; Zhu, Y.; Shao, S.; Zhang, R.; Wu Y.; Zhu, C.; Liang, X.; Cai, W. Alkyl ferulate esters as multi-functional food additives: antibacterial activity and mode of action against *Escherichia coli* in Vitro. *J. Agric. Food Chem.* **2018**, *66*, 12088-12101.

[11] Shi, Y.; Bian L.; Zhu Y.; Zhang, R.; Shao, S.; Wu, Y.; Chen, Y.; Dang, Y.; Sun, H. Multifunctional alkyl ferulate esters as potential food additives: Antibacterial activity and mode of action against *Listeria monocytogenes* and its application on American sturgeon caviar preservation. *Food Control.* **2019**, *96*, 390-402.

[12] Wu, Y.; Shi, Y.; Zheng, X.; Dang, Y.; Zhu, C.; Zhang, R.; Fu, Y.; Zhou, T.; Li, J. Lipophilic ferulic acid derivatives protect PC12 cells against oxidative damage: Via modulating β-amyloid aggregation and activating Nrf2 enzymes. *Food Funct.* **2020**, *11*, 4707-4718.

[13] Shi, Y.; Zhang, R.; Zhu, C.; Xu, M.; Gu, Q.; Ettelaie, R.; Lin, S.; Wang, Y.; Leng. X. Antimicrobial mechanism of alkyl gallates against *Escherichia coli* and *Staphylococcus aureus* and its combined effect with electrospun nanofibers on Chinese Taihu icefish preservation. *Food Chem*. **2021**, *346*, 128949.

[14] Sivasankaran, U.; Vikraman, A. E.; Thomas, D.; Kumar, K. G. Nanomolar level determination of octyl gallate in fats and oils. *Food Anal. Method.* **2016**, *9*, 2115-2123.

[15] Jeon, M. J.; Ha, J. W. Inactivating Foodborne Pathogens in Apple Juice by Combined Treatment with Fumaric Acid and Ultraviolet-A Light, and Mechanisms of Their Synergistic Bactericidal Action. *Food Microbiol.* **2020**, *87* 103387.

[16] Supaphol, P.; Suwantong, O.; Sangsanoh, P.; Srinivasan, S.; Jayakumar, R.; Nair, S. V. Electrospinning of Biocompatible Polymers and Their Potentials in Biomedical Applications. *Biomed. Appl. Polym. Nanofiber*. **2012**, *246*, 213-239.

[17] Xue, J.; Wu, T.; Dai, Y.; Xia, Y. Electrospinning and Electrospun Nanofibers: Methods, Materials, and Applications. *Chem Rev*. **2019**, *119*, 5298-5415.

[18] Hemp, S. T.; Hudson, A. G.; Allen, M. H.; Pole, S. S.; Moore, R. B.; Long, T. E. Solution Properties and Electrospinning of Phosphonium Gemini Surfactants. *Soft Matter*. **2014**, *10*, 3970-3977.

[19] Jansook, P.; Ogawa, N.; Loftsson, T. Cyclodextrins: structure, physicochemical properties and pharmaceutical applications. *Int. J. Pharm*. **2018**, *535*, 272-284.

[20] Yildiz, Z. I.; Kilic, M. E.; Durgun, E.; Uyar, T. Molecular Encapsulation of Cinnamaldehyde within Cyclodextrin Inclusion Complex Electrospun Nanofibers: Fast-Dissolution, Enhanced Water Solubility, High Temperature Stability, and Antibacterial Activity of Cinnamaldehyde. *J. Agric. Food Chem.* **2019**, *67*, 11066-11076.

[21] Chen, J.; Song, M.; Wu, X.; Zheng, J.; He, L.; McClements, D. J.; Decker, E.; Xiao, H. Direct Fluorescent Detection of a Polymethoxyflavone in Cell Culture and Mouse Tissue. *J. Agric. Food Chem.* **2015**, *63*, 10620-10627.

[22] Wang, Q.; Oliveira, E. F.; Alborzi, S.; Bastarrachea, L. J. On mechanism behind UV-A light enhanced antibacterial activity of gallic acid and propyl gallate against *Escherichia coli* O157:H7. *Sci Rep*. **2017**, 7, 8325.

[23] Zhang, Q. Z.; Zhao, K. Q.; Wu, Y.; Li, X. H.; Yang, C.; Guo, L. M.; Liu, C. H.; Qu, D.; Zheng, C. Q. 5-Aminolevulinic Acid-Mediated Photodynamic Therapy and Its Straindependent Combined Effect with Antibiotics on *Staphylococcus Aureus* Biofilm. *PLoS One.* **2017**, *12*, 1-12.

[24] Price, M.; Reiners, J. J.; Santiago, A. M.; Kessel, D. Monitoring Singlet Oxygen and Hydroxyl Radical Formation with Fluorescent Probes during Photodynamic Therapy. *Photochem. Photobiol.* **2009**, *85*, 1177-1181.

[25] Celebioglu, A.; Uyar, T. Fast Dissolving Oral Drug Delivery System Based on Electrospun Nanofibrous Webs of Cyclodextrin/Ibuprofen Inclusion Complex Nanofibers. *Mol. Pharm.* **2019**, *16*, 4387-4398.

[26] Pu, H.; Sun, Q.; Tang, P.; Zhao, L.; Li, Q.; Liu, Y.; Li, H. Characterization and antioxidant activity of the complexes of tertiary butylhydroquinone with β-cyclodextrin and its derivatives. *Food Chem.* **2018**, *260*, 183-192.

[27] Cossu, A.; Ercan, D.; Wang, Q.; Peer, W. A.; Nitin, N.; Tikekar, R. V. Antimicrobial Effect of Synergistic Interaction between UV-A Light and Gallic Acid against *Escherichia Coli* O157:H7 in Fresh Produce Wash Water and Biofilm. *Innov. Food Sci. Emerg. Technol.* **2016**, *37*, 44-52.

[28] Nakamura, K.; Ishiyama, K.; Sheng, H.; Ikai, H.; Kanno, T.; Niwano, Y. Bactericidal Activity and Mechanism of Photoirradiated Polyphenols against Gram-Positive and -Negative Bacteria. *J. Agric. Food Chem.* **2015**, *63*, 7707-7713.

[29] Kubo, I.; Fujita, K.; Nihei, K.; Nihei, A. Antibacterial activity of alkyl gallates against *bacillus subtilis*. *J. Agric. Food Chem.* ***2004***, *52*, 1072-1076.

[30] Arakawa, H.; Maeda, M.; Okubo, S.; Shimamura, T. Role of Hydrogen Peroxide in Bactericidal Action of Catechin. *Biol. Pharm. Bull.* **2004**, *27*, 277-281.

[31] Akagawa, M.; Shigemitsu, T.; Suyama, K. Production of Hydrogen Peroxide by Polyphenols and Polyphenol-Rich Beverages under Quasi-Physiological Conditions. *Biosci. Biotechnol. Biochem.* **2003**, *67*, 2632-2640.

[32] Long, L. H.; Clement, M. V.; Halliwell, B. Artifacts in Cell Culture: Rapid Generation of Hydrogen Peroxide on Addition of (−)-Epigallocatechin, (−)-Epigallocatechin Gallate, (+)-Catechin, and Quercetin to Commonly Used Cell Culture Media. *Biochem. Biophys. Res. Commun.* **2000**, *273*, 50-53.

[33] Wang, Q.; Leong, W. F.; Elias, R. J.; Tikekar, R. V. UV-C irradiated gallic acid exhibits enhanced antimicrobial activity via generation of reactive oxidative species and quinone. *Food Chem*. **2019**, 287, 303-312.

[34] Mochizuki, M.; Yamazaki, S. I.; Kano, K.; Ikeda, T. Kinetic Analysis and Mechanistic Aspects of Autoxidation of Catechins. *Biochim. Biophys. Acta-Gen. Subj.* **2002**, *1569*, 35-44.

[35] Shirato, M.; Ikai, H.; Nakamura, K.; Hayashi, E.; Kanno, T.; Sasaki, K.; Kohno, M.; Niwano, Y. Synergistic Effect of Thermal Energy on Bactericidal Action of Photolysis of H_2O_2 in Relation to Acceleration of Hydroxyl Radical Generation. *Antimicrob. Agents Chemother.* **2012**, *56*, 295-301.

[36] Nakamura, K.; Yamada, Y.; Ikai, H.; Kanno, T.; Sasaki, K.; Niwano, Y. Bactericidal action of photoirradiated gallic acid via reactive oxygen species formation. *J. Agric. Food Chem.* **2012**, *60*, 10048-10054.

[37] Kanno, T.; Nakamura, K.; Ikai, H.; Hayashi, E.; Shirato, M.; Mokudai, T.; Iwasawa, A.; Niwano, Y.; Kohno, M.; Sasaki, K. Novel denture cleaning system based on hydroxyl radical disinfection. *Int. J. Prosthodont.* **2012**, 25, 376-380.

[38] Setsukinai, K. ichi; Urano, Y.; Kakinuma, K.; Majima, H. J.; Nagano, T. Development of Novel Fluorescence Probes That Can Reliably Detect Reactive Oxygen Species and Distinguish Specific Species. *J. Biol. Chem.* **2003**, *278*, 3170-3175.

[39] Lacombe, A.; Wu, V. C. H.; Tyler, S.; Edwards, K. Antimicrobial Action of the American Cranberry Constituents; Phenolics, Anthocyanins, and Organic Acids, against *Escherichia Coli* O157:H7. *Int. J. Food Microbiol.* **2010**, *139*, 102-107.

[40] Stiefel, P.; Schmidt-Emrich, S.; Maniura-Weber, K.; Ren, Q. Critical Aspects of Using Bacterial Cell Viability Assays with the Fluorophores SYTO9 and Propidium Iodide. *BMC Microbiol.* **2015**, *15*, 1-9.

[41] Kubo, I.; Fujita, K.; Nihei, K. Anti-Salmonella activity of alkyl gallates. *J. Agric. Food Chem.*

2002, *50*, 6692-6696.

[42] Park, H.-J.; Kim, J. Y.; Kim, J.; Lee, J.-H.; Hahn, J.-S.; Gu, M. B.; Yoon, J. Silver-Ion-Mediated Reactive Oxygen Species Generation Affecting Bactericidal Activity. *Water Res.* **2009**, *43*, 1027-1032.

[43] Ou, S.; Wang, Y.; Tang, S.; Huang, C.; Jackson, M. G. Role of Ferulic Acid in Preparing Edible Films from Soy Protein Isolate. *J. Food Eng.* **2005**, *70*, 205-210.

[44] Huang, J.; Chen, B.; Li, H.; Zeng, Q.; Wang, J.; Liu, H.; Pan, Y.; Zhao, Y. Enhanced antibacterial and antibiofilm functions of the curcumin-mediated photodynamic inactivation against *Listeria monocytogenes*. *Food Control*. **2020**, *108*, 106886.

[45] Almeida, A.; Faustino, M. AF.; Tome, J. PC. Photodynamic inactivation of bacteria: finding the effective targets. *Future Med. Chem.* **2015**, *7*, 1221-1224.

[46] Higuchi, T.; Connors, K. A. Advances in analytical chemistry and instrumentation. *Phase solubility techniques.* **1965**, *4*, 117-122.

[47] Uyar, T.; Besenbacher, F. Electrospinning of Uniform Polystyrene Fibers: The Effect of Solvent Conductivity. *Polymer (Guildf).* **2008**, *49*, 5336-5343.

[48] da Rosa, C.G.; Borges, C. D.; Zambiazi, R. C.; Nunes, M. R.; Benvenutti, E. V.; da Luz, S.; D'Avila, R. F.; Rutz, J. K. Microencapsulation of gallic acid in chitosan, β-cyclodextrin and xanthan. *Ind. Crop. Prod*. **2013**, *46*, 138-146.

TABLES and FIGURE Legends

Figure 1. Evaluate the effect of OG concentration and UV-A light irradiation time on the antimicrobial activity in the absence or presence of UV-A at 25 ^{o}C. The number of bacteria in the suspension was determined by standard plate counting. (**A**) OG concentration-dependent bactericidal activity (treatment time: 30 min). (**B**) The effect of irradiation treatment time on the bactericidal activity of OG-mediated PDI. (**C**) Time-dependent photodynamic bactericidal activity of either OG or GA against *E. coli* (**a**) and *S. aureus* (**b**). Wavelength: 365 nm, irradiance: 8.254±0.18 mW/cm^2. Values and error bars indicate the mean and standard deviation, respectively. Significant differences are shown, P<0.05 (*) and P<0.01 (**). ND: not detected. OG: octyl gallate; GA: gallic acid; NS: normal saline.

Figure 2. (**A**) Uptake of either OG or GA in *E. coli* as measured by the combination with diphenylboric acid 2-aminoethyl ester (DPBA). *E. coli* treated by OG or GA (0.15 mM) solution in the presence and absence of UV-A light for 30 min. Absolute fluorescence values were corrected by subtracting the fluorescence values for samples incubated in water and in dark. (**B**) Confocal laser scanning microscopy images of GA or OG in *E. coli* stained with DPBA.

Figure 3. Measurement of oxidative stress experienced by *E. coli* by the different treatments. (**A**) Total reactive oxygen species were detected using DCFH-DA in *E. coli* treated by either OG or GA (0.15 mM) solution in the presence and absence of UV-A light. DCFH-DA was used for measuring intracellular oxidative stress in cells because it can be oxidized to green fluorescent 2',7'-dichlorofluorescein (DCF) by cytosolic ROS. Values and error bars indicate the mean and standard deviation, respectively. Significant differences (P<0.05) between the groups are denoted by different superscript letters. (**B**) CLSM images of *E. coli* incubated with DCFH-DA. Photodynamic inactivation of *E. coli* was evaluated at 37 °C in presence of OG (0.15 mM) and simultaneously illuminated by UV-A for 30 min (DIC-differential interference contrast). Pictures were taken using ×63 oil immersion lens with a zoom factor of 2. (**C**) Detection of intracellular reactive oxygen species using DCFH-DA within *E. coli* with or without scavengers including CAT (600 U/mL), DMSO (1.0 M), or TEMPOL (8 mM). Values and error bars indicate the mean and standard deviation, respectively. Significant differences (P<0.05) between the groups are denoted by different superscript letters. (**D**) Antibacterial assessments of OG+UV-A with or without CAT (600 U/mL), DMSO (1.0 M), or TEMPOL (8 mM). A mixture of bacterial suspension and OG solution (0.15 mM) was irradiated with UV-A light for 15 min. Values and error bars indicate the mean and standard deviation, respectively. Significant differences (P<0.05) between the groups are denoted by different superscript letters. (**E**) Generation of hydroxyl radicals in *E. coli* treated by OG

(0.15 mM) solution in the presence and absence of UV-A light.

Figure 4. (**A**) Membrane damage as indicated by the fluorescence level of PI in *E. coli* treated by OG or GA solution with or without UV-A irradiation. The initial bacterial density of *E. coli* is ~10^8 CFU/mL. (**B**) Scanning electron microscopy (SEM) images of *E. coli*. (a), (b) and (c) were SEM images of control, treatment by OG, and OG+UV-A for 30 min, respectively. (**C**) Effects of OG-mediated PDI on the total proteins of *E. coli*. (**D**) FTIR spectrums of membrane proteins from *E. coli*. (**E**) Effects of the OG-mediated PDI on the genomic DNA of *E. coli*. *E. coli* treated by OG solution with the final concentration of 0.15 mM with or without UV-A irradiation. Wavelength: 365 nm, irradiance: 8.254±0.18 mW/cm^2, treatment time: 30 min.

Figure 5. (A) The representative SEM images and the fiber diameter distribution graphs of electrospun fibers from (a) pure HP*β*CD NFs and (b) OG/HP*β*CD NFs (1:1). The insets show the high magnification images. **(B)** ^{1}H NMR spectra of pure HP*β*CD NFs, OG, and OG/HP*β*CD NFs (1:1). The ^{1}H NMR spectra were recorded by dissolving the samples in DMSO-d_6. The characteristic peaks of HP*β*CD and OG are highlighted in blue and red colors, respectively. (**C**) FTIR spectrums of OG, pure HP*β*CD NFs, and OG/HP*β*CD (1:1) NFs. (**D**) XRD patterns of OG, pure HP*β*CD NFs, and OG/HP*β*CD (1:1) NFs. (**E**) DSC thermograms of OG, pure HP*β*CD NFs, and OG/HP*β*CD (1:1) NFs.

Figure 6. **(A**) Results of bactericidal assessments in the group treated with OG/HP*β*CD NFs against 6 Log CFU/mL bacteria under UV-A exposure for (**a**) 30 min, and (**b**) the impact of irradiation time on the bactericidal effect. Significant differences (P<0.05) between the groups are denoted by different letters. (**B**) The situ photodynamic antibacterial effect of OG/HP*β*CD NFs with UV-A irradiation for 5 min on Chinese giant salamander. ND: not detected. Significant differences (P<0.05) between the groups are denoted by different letters. (**C**) The change of colonies of Chinese giant salamander after storage for 3, 6, 9, 12, and 15 days at 4 ^{o}C. The fresh salamander meat was packed using OG/HP*β*CD NFs and then immediately treated with UV-A irradiation for 5 min. (**D**) The PCA of Chinese giant salamander with different treatments: (a) fresh salamander meat; (b) control; (c) only UV-A; (d) only OG/HP*β*CD NFs; (e) OG/HP*β*CD NFs + UV-A (b-e, 4 ^{o}C, 15 days). The salamander meat was singly sealed with OG/HP*β*CD NFs and irradiated immediately with UV-A light for 5 min.

892 **SCHEME**

893

894 *Shi et al.*

895

896

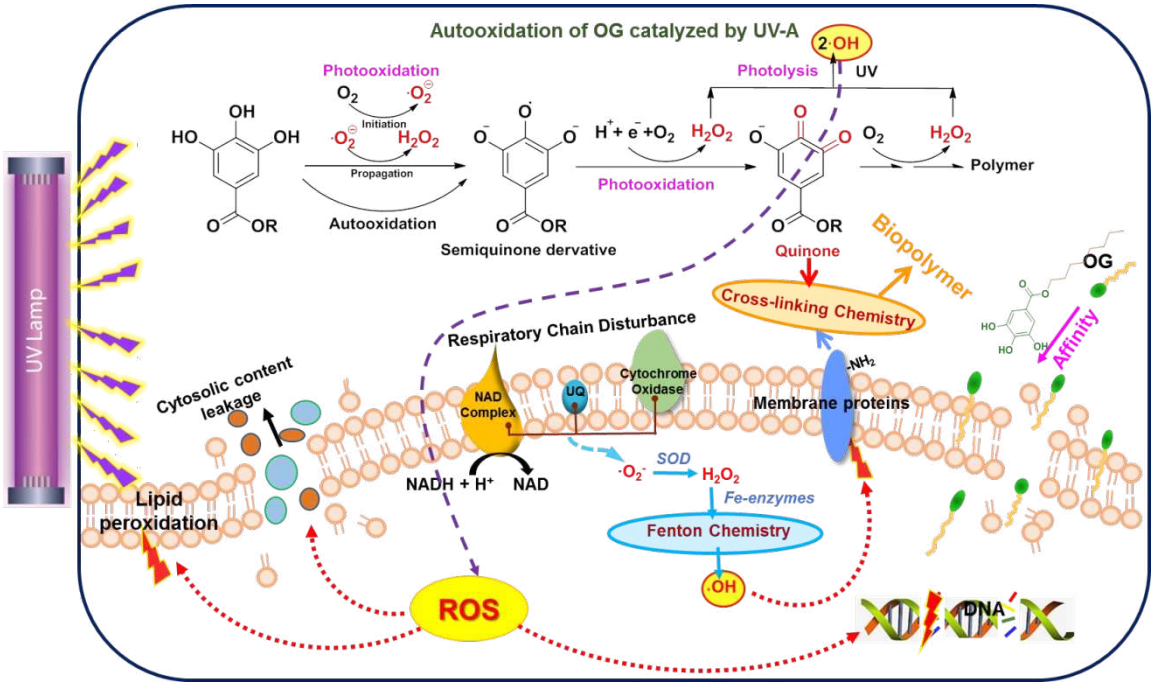

897

898

899 **Scheme 1.** Proposed multi-mechanism of the OG-mediated photodynamic inactivation (PDI). (1)
900 OG facilely permeates into the cells and damages the bacterial membrane and then (2) disrupts the
901 activity of ETC on the cytoplasmic membrane to generate a high level of toxic ROS. (3) Besides,
902 the polyphenolic hydroxyl group of OG would be oxidized by the photoradiation to induce ROS
903 generation. ROS would cause lethal oxidative damage to bacteria. (4) Quinone intermediates
904 generated from OG-mediated PDI could react with amino or sulfhydryl side chains of membrane
905 proteins through the cross-linking chemistry, manifesting greater bactericidal activity.

906

907

908

FIGUREs

Shi et al.

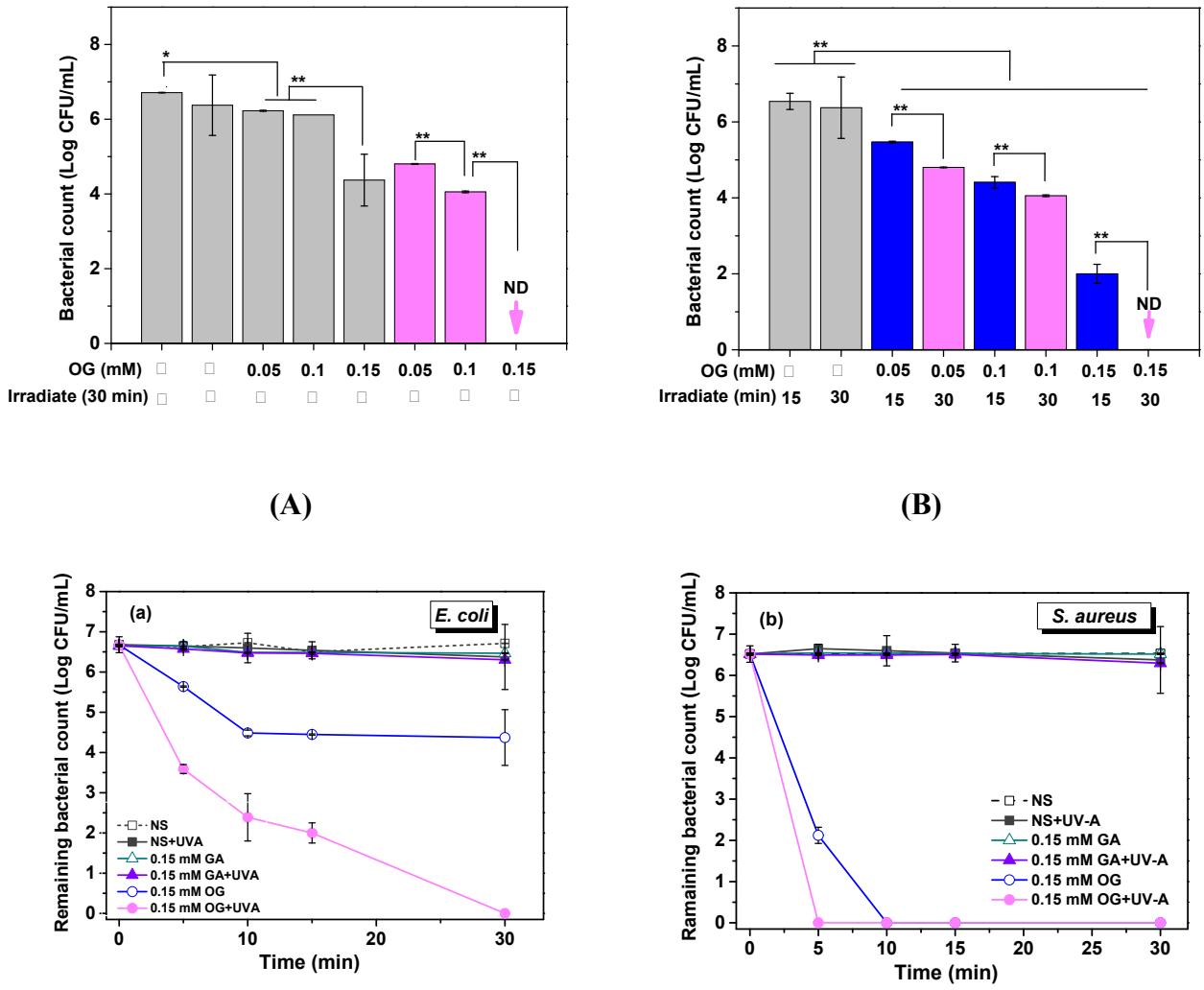

Figure 1. Evaluate the effect of OG concentration and UV-A light irradiation time on the antimicrobial activity in the absence or presence of UV-A at 25 °C. The number of bacteria in the suspension was determined by standard plate counting. (**A**) OG concentration-dependent bactericidal activity (treatment time: 30 min). (**B**) The effect of irradiation treatment time on the bactericidal activity of OG-mediated PDI. (**C**) Time-dependent photodynamic bactericidal activity of either OG or GA against *E. coli* (**a**) and *S. aureus* (**b**). Wavelength: 365 nm, irradiance: 8.254±0.18 mW/cm^2. Values and error bars indicate the mean and standard deviation, respectively.

920 Significant differences are shown, $P<0.05$ (*) and $P<0.01$ (**). ND: not detected. OG: octyl gallate;
921 GA: gallic acid; NS: normal saline.
922
923

924 *Shi et al.*

925

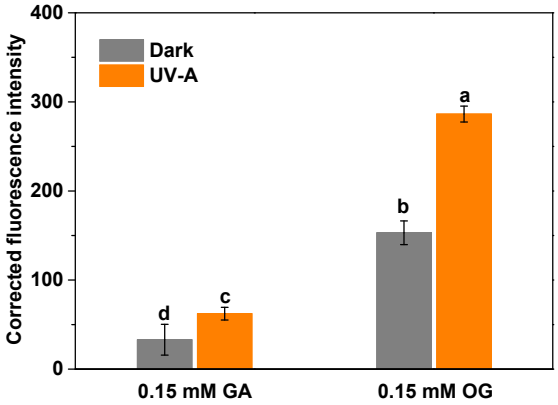

926

927 **(A)**

928

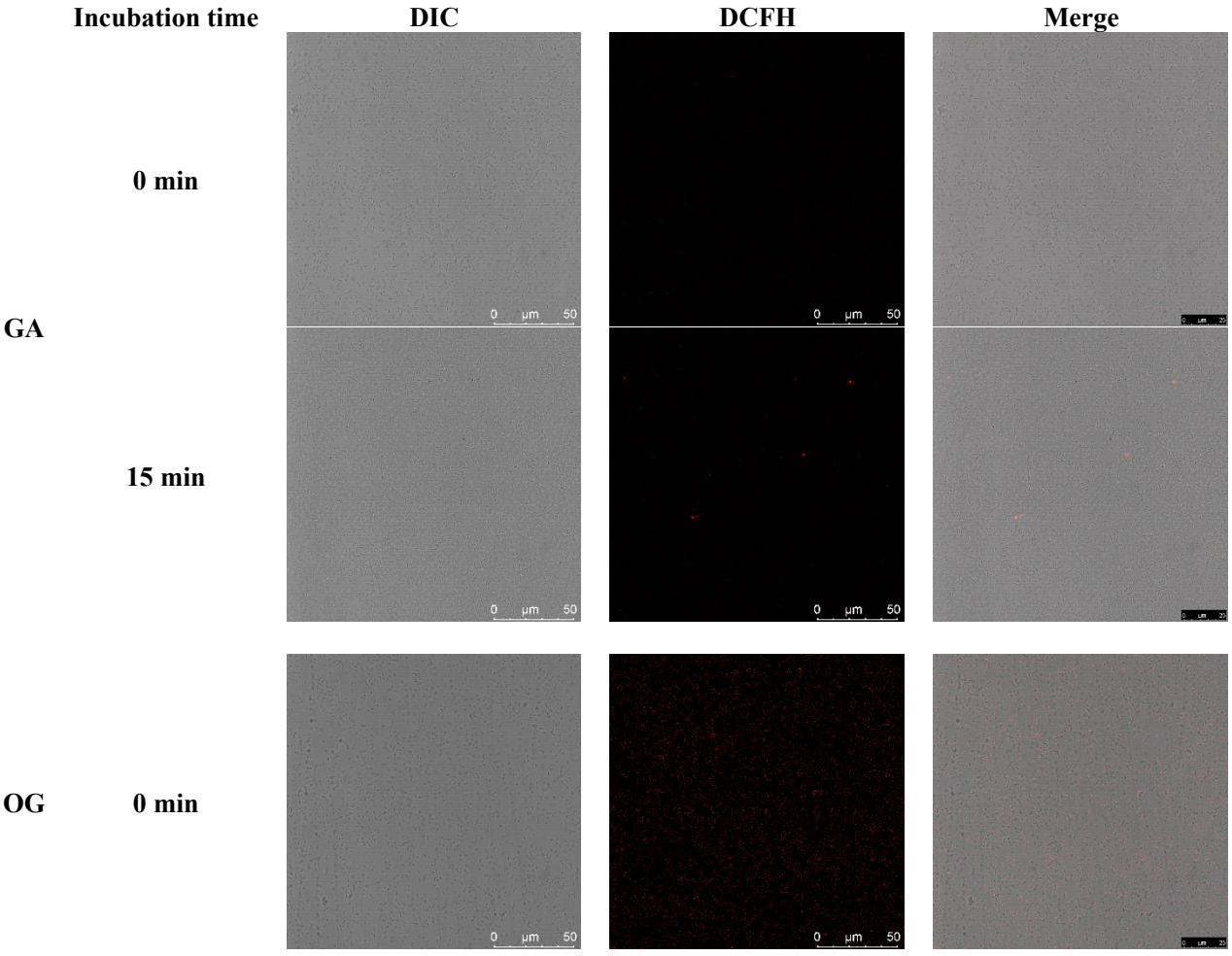

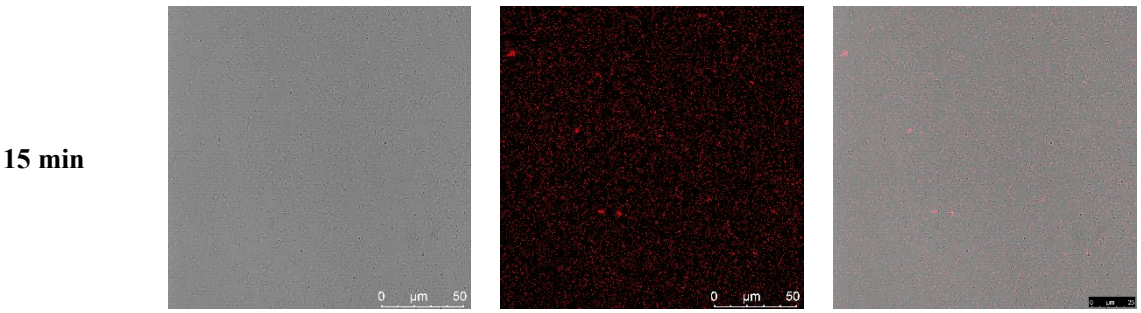

(B)

Figure 2. (**A**) Uptake of either OG or GA in *E. coli* as measured by the combination with diphenylboric acid 2-aminoethyl ester (DPBA). *E. coli* treated by OG or GA (0.15 mM) solution in the presence and absence of UV-A light for 30 min. Absolute fluorescence values were corrected by subtracting the fluorescence values for samples incubated in water and in dark. (**B**) Confocal laser scanning microscopy images of GA or OG in *E. coli* stained with DPBA.

937 *Shi et al.*

938

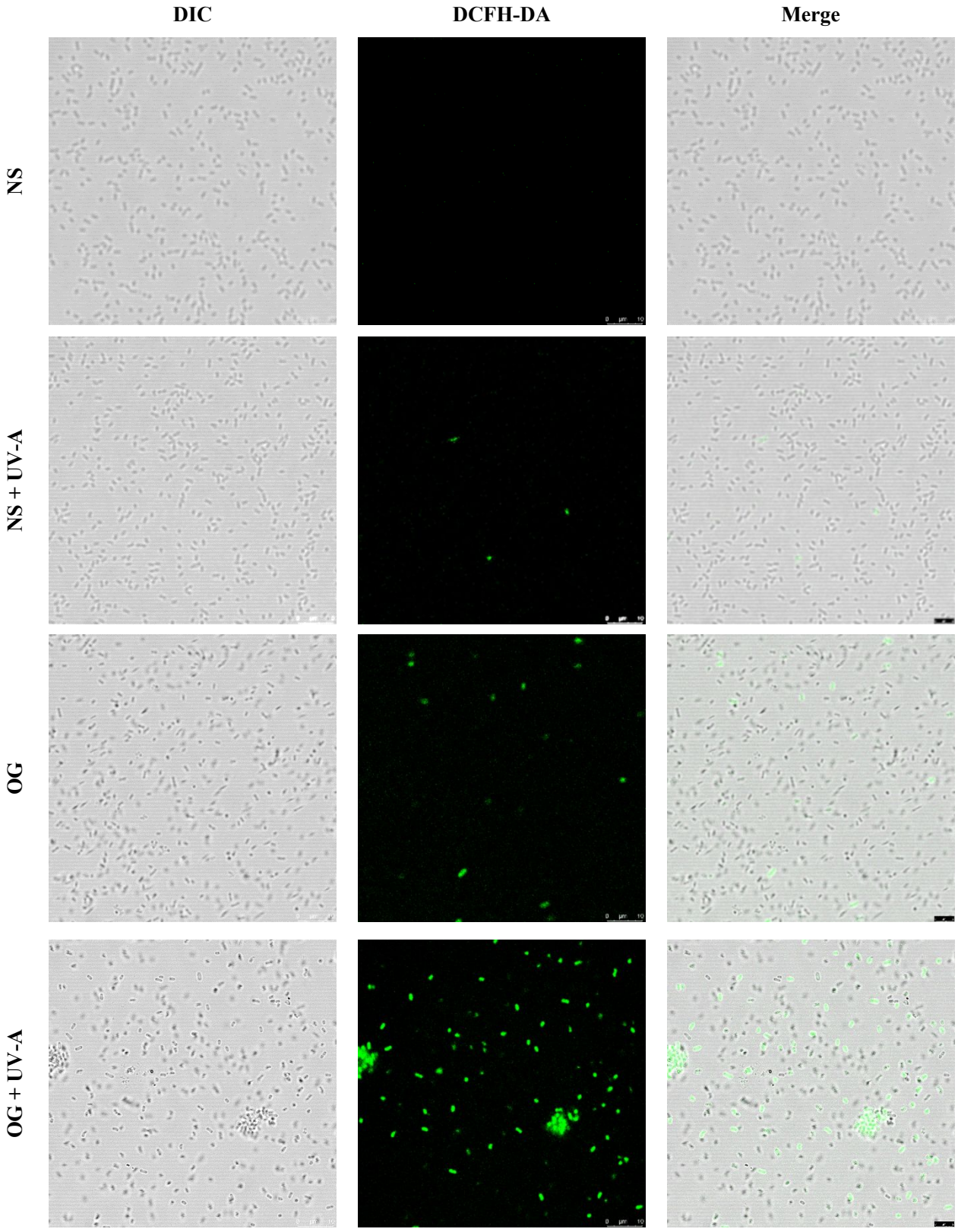

(B)

939

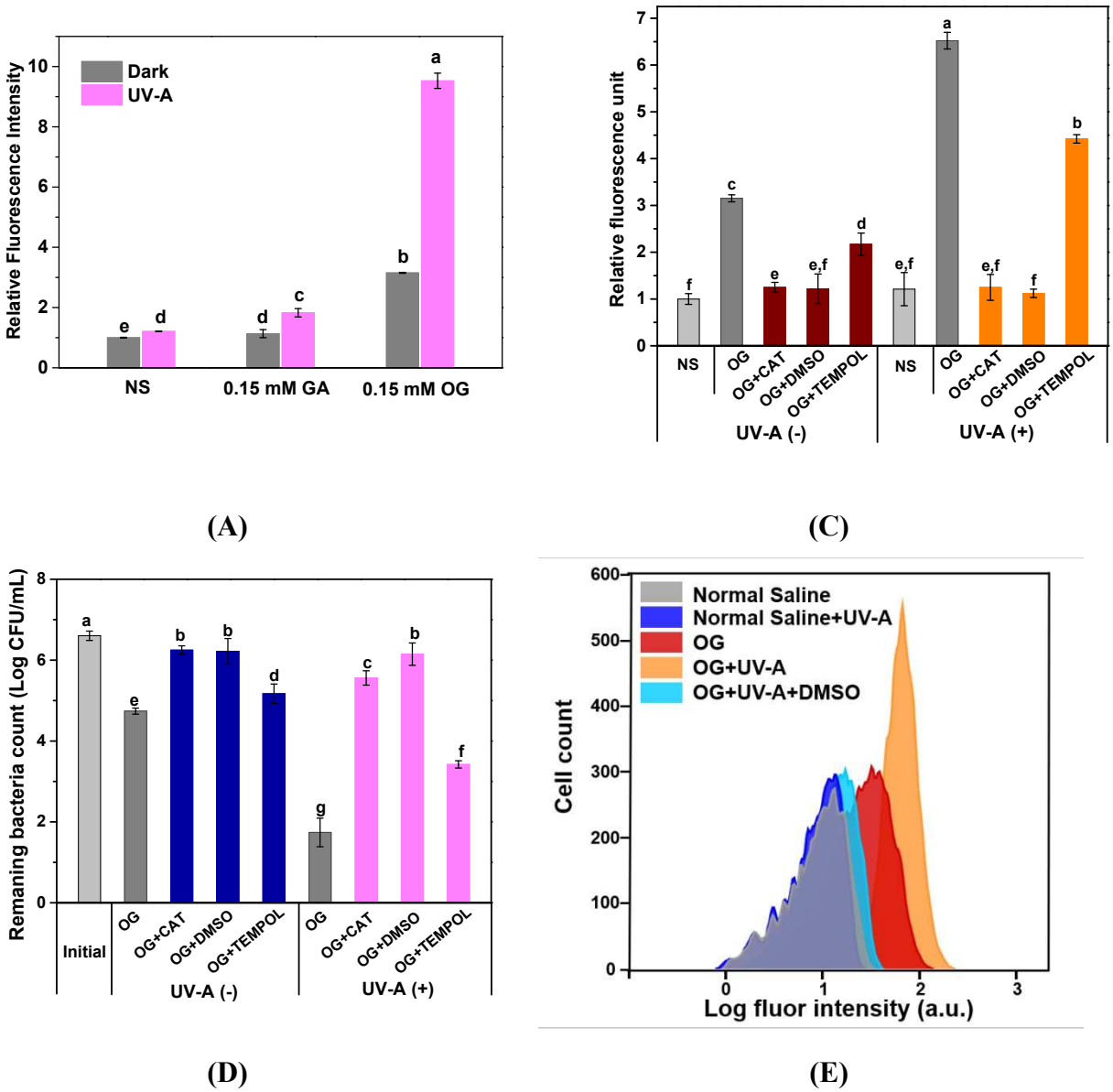

940

941 **Figure 3.** Measurement of oxidative stress experienced by *E. coli* by the different treatments. (**A**)
942 Total reactive oxygen species were detected using DCFH-DA in *E. coli* treated by either OG or GA
943 (0.15 mM) solution in the presence and absence of UV-A light. DCFH-DA was used for measuring
944 intracellular oxidative stress in cells because it can be oxidized to green fluorescent
945 2',7'-dichlorofluorescein (DCF) by cytosolic ROS. Values and error bars indicate the mean and
946 standard deviation, respectively. Significant differences (P<0.05) between the groups are denoted
947 by different superscript letters. (**B**) CLSM images of *E. coli* incubated with DCFH-DA.
948 Photodynamic inactivation of *E. coli* was evaluated at 37 °C in presence of OG (0.15 mM) and
949 simultaneously illuminated by UV-A for 30 min (DIC-differential interference contrast). Pictures
950 were taken using ×63 oil immersion lens with a zoom factor of 2. (**C**) Detection of intracellular
951 reactive oxygen species using DCFH-DA within *E. coli* with or without scavengers including CAT

952 (600 U/mL), DMSO (1.0 M), or TEMPOL (8 mM). Values and error bars indicate the mean and
953 standard deviation, respectively. Significant differences (P<0.05) between the groups are denoted
954 by different superscript letters. (**D**) Antibacterial assessments of OG+UV-A with or without CAT
955 (600 U/mL), DMSO (1.0 M), or TEMPOL (8 mM). A mixture of bacterial suspension and OG
956 solution (0.15 mM) was irradiated with UV-A light for 15 min. Values and error bars indicate the
957 mean and standard deviation, respectively. Significant differences (P<0.05) between the groups are
958 denoted by different superscript letters. (**E**) Generation of hydroxyl radicals in *E. coli* treated by OG
959 (0.15 mM) solution in the presence and absence of UV-A light.
960
961

962 *Shi et al.*

963

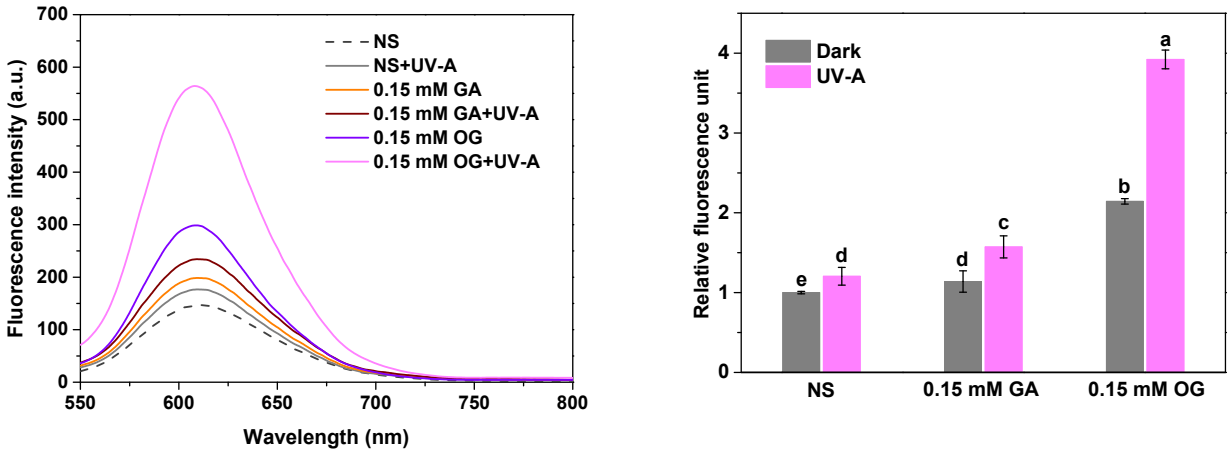

(A)

964

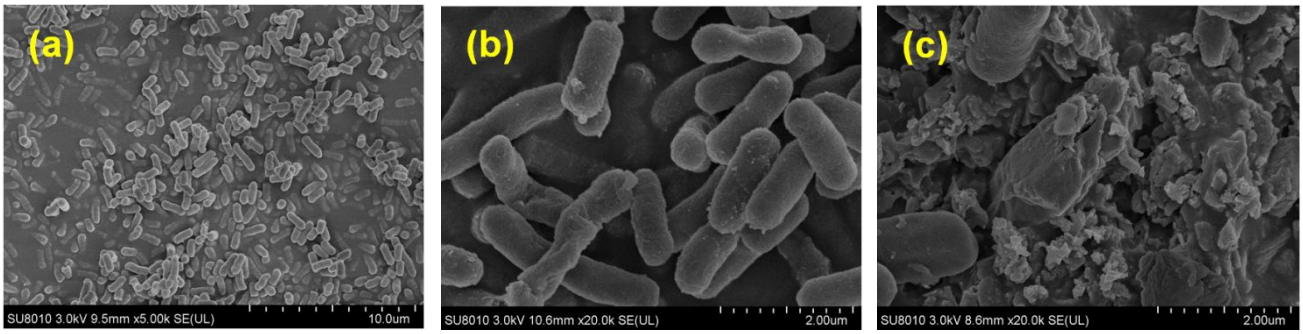

(B)

965

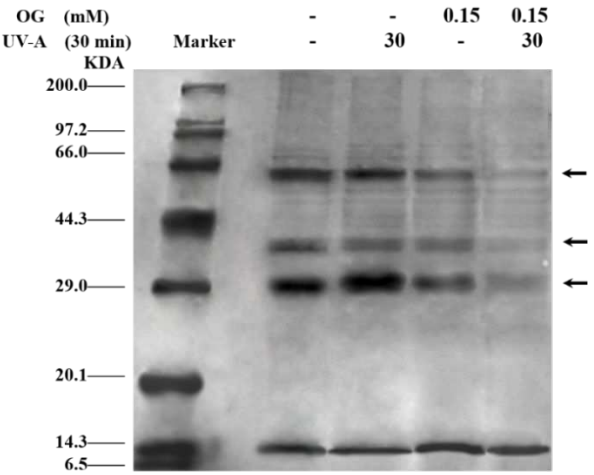

(C)

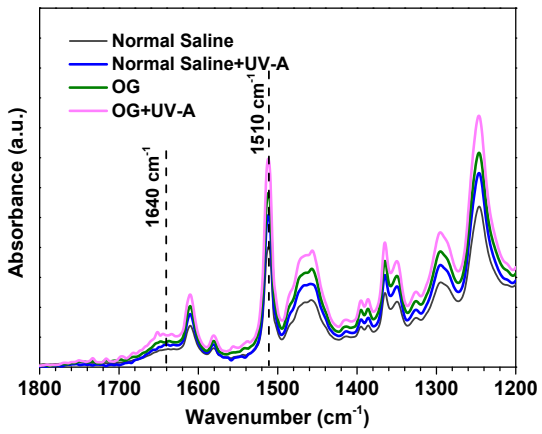

(D)

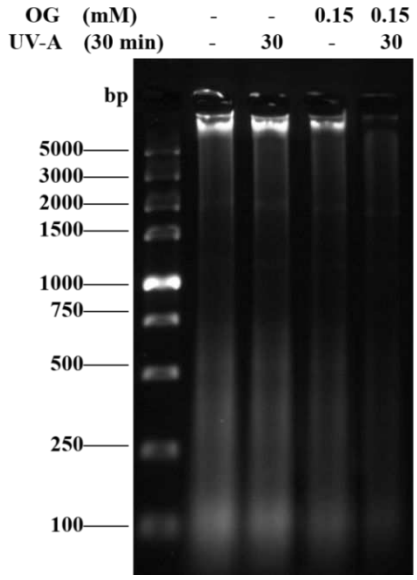

(E)

Figure 4. (**A**) Membrane damage as indicated by the fluorescence level of PI in *E. coli* treated by OG or GA solution with or without UV-A irradiation. The initial bacterial density of *E. coli* is ~10^8 CFU/mL. (**B**) Scanning electron microscopy (SEM) images of *E. coli*. (a), (b) and (c) were SEM images of control, treatment by OG, and OG+UV-A for 30 min, respectively. (**C**) Effects of OG-mediated PDI on the total proteins of *E. coli*. (**D**) FTIR spectrums of membrane proteins from *E. coli*. (**E**) Effects of the OG-mediated PDI on the genomic DNA of *E. coli*. *E. coli* treated by OG solution with the final concentration of 0.15 mM with or without UV-A irradiation. Wavelength: 365 nm, irradiance: 8.254±0.18 mW/cm^2, treatment time: 30 min.

977 *Shi et al.*

978

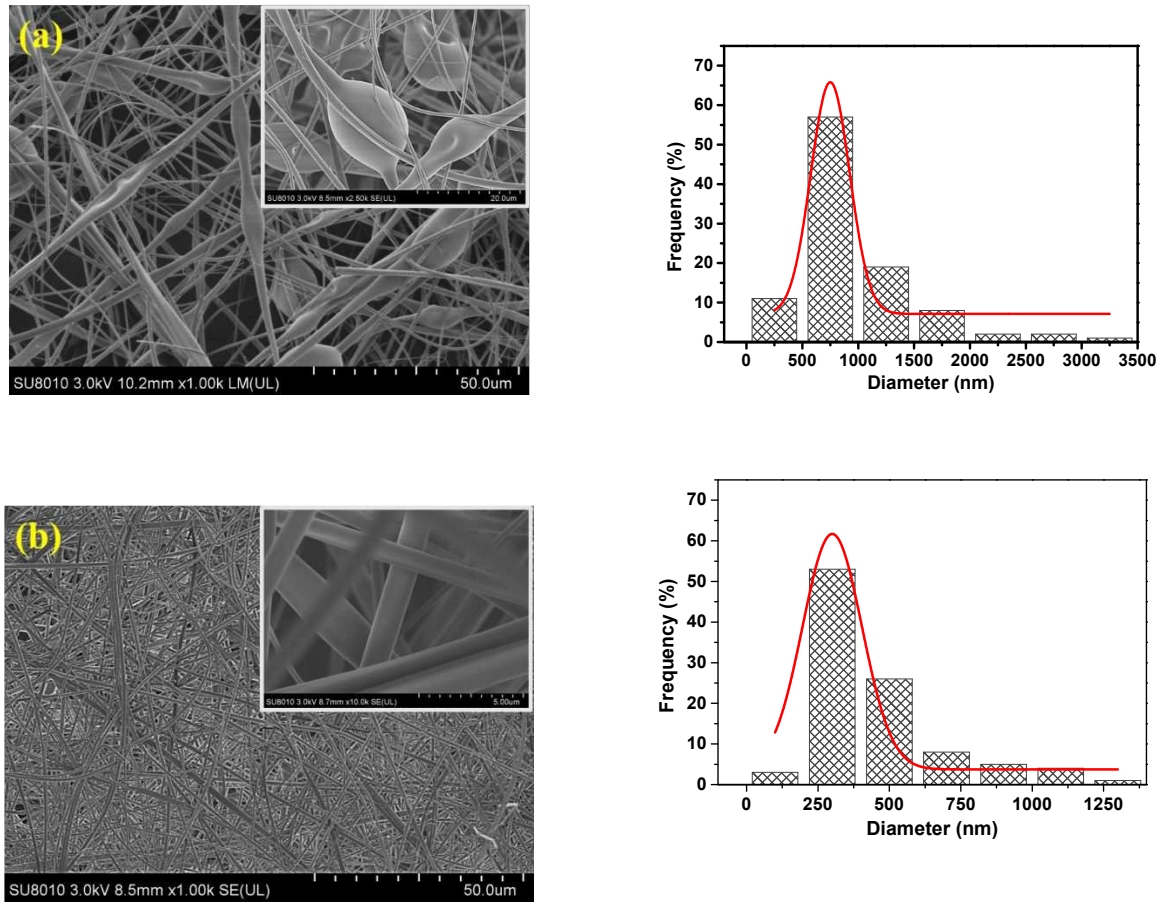

(A)

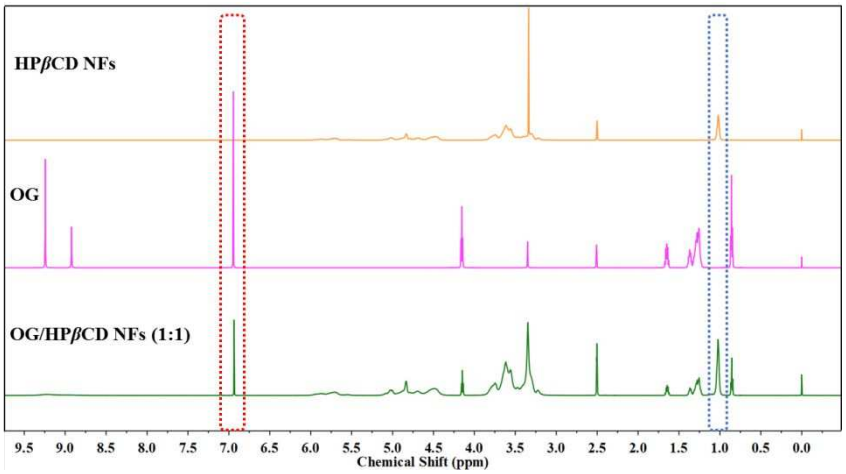

(B)

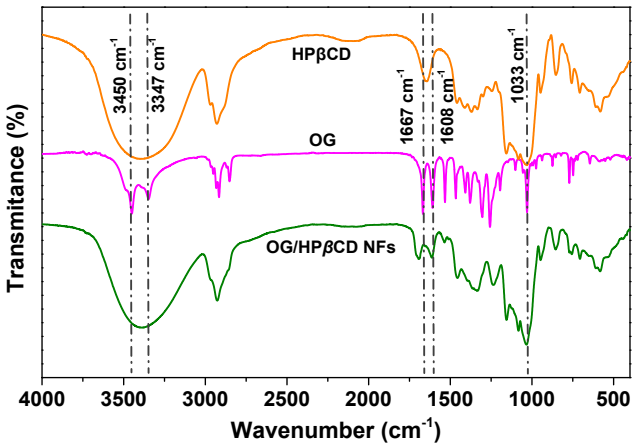

(C)

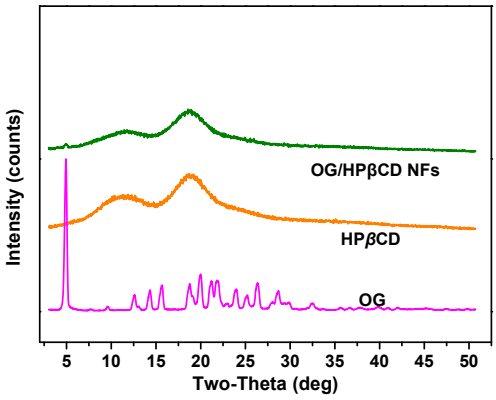

(D)

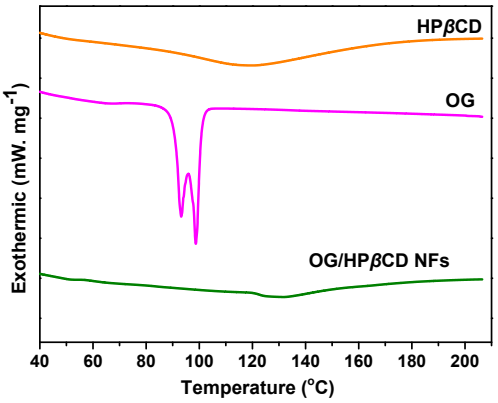

(E)

Figure 5. (A) The representative SEM images and the fiber diameter distribution graphs of electrospun fibers from (a) pure HP*β*CD NFs and (b) OG/HP*β*CD NFs (1:1). The insets show the high magnification images. **(B)** ^{1}H NMR spectra of pure HP*β*CD NFs, OG, and OG/HP*β*CD NFs (1:1). The ^{1}H NMR spectra were recorded by dissolving the samples in DMSO-d_6. The characteristic peaks of HP*β*CD and OG are highlighted in blue and red colors, respectively. (**C**) FTIR spectrums of OG, pure HP*β*CD NFs, and OG/HP*β*CD (1:1) NFs. (**D**) XRD patterns of OG, pure HP*β*CD NFs, and OG/HP*β*CD (1:1) NFs. (**E**) DSC thermograms of OG, pure HP*β*CD NFs, and OG/HP*β*CD (1:1) NFs.

989 *Shi et al.*

990

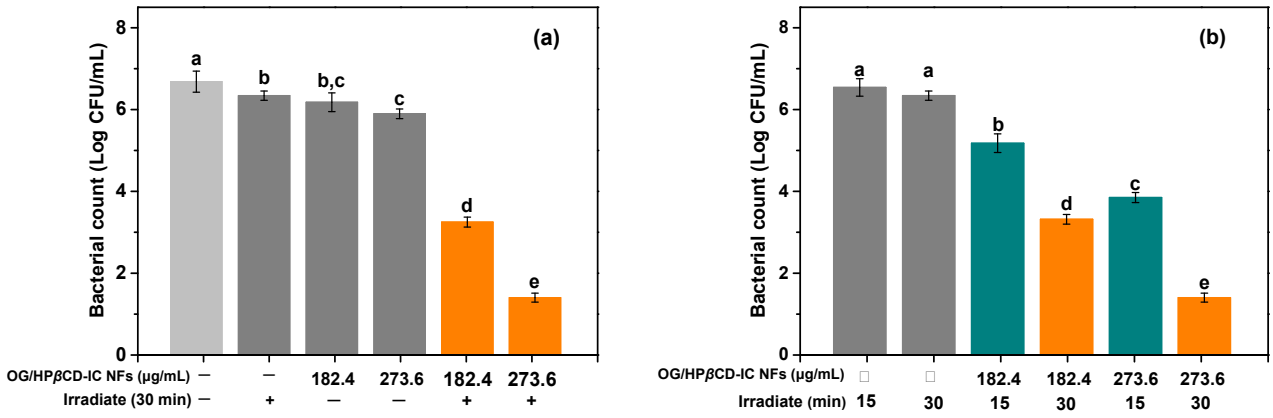

(A)

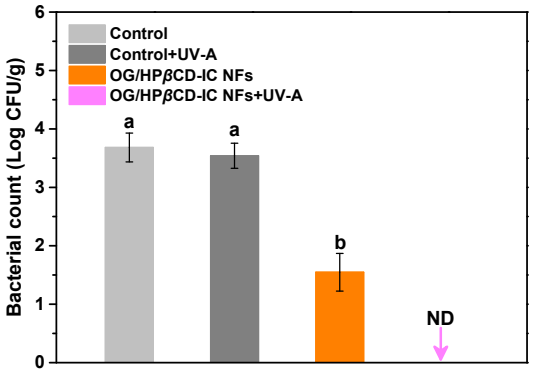

(B)

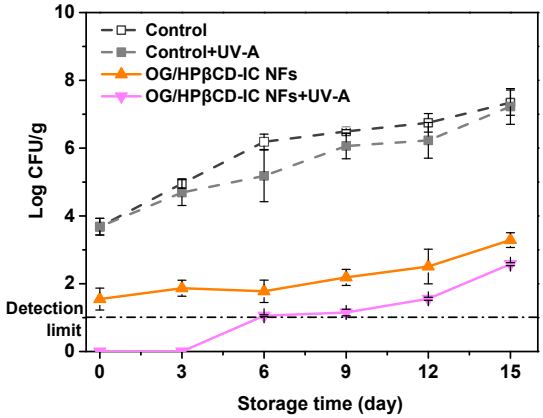

(C)

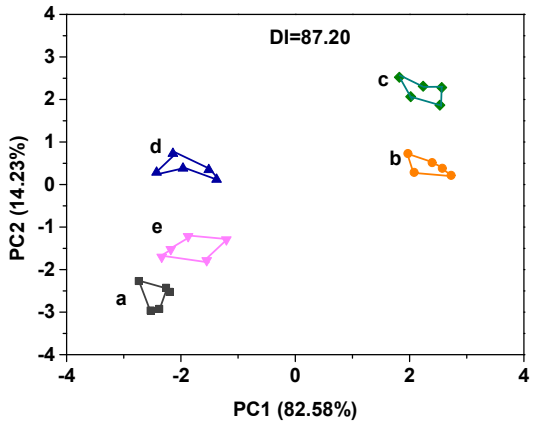

(D)

991

992 **Figure 6**. **(A)** Results of bactericidal assessments in the group treated with OG/HP*β*CD NFs against
993 6 Log CFU/mL bacteria under UV-A exposure for (**a**) 30 min, and (**b**) the impact of irradiation time
994 on the bactericidal effect. Significant differences (P<0.05) between the groups are denoted by
995 different letters. (**B**) The situ photodynamic antibacterial effect of OG/HP*β*CD NFs with UV-A
996 irradiation for 5 min on Chinese giant salamander. ND: not detected. Significant differences
997 (P<0.05) between the groups are denoted by different letters. (**C**) The change of colonies of Chinese
998 giant salamander after storage for 3, 6, 9, 12, and 15 days at 4 ^{o}C. The fresh salamander meat was
999 packed using OG/HP*β*CD NFs and then immediately treated with UV-A irradiation for 5 min. (**D**)
1000 The PCA of Chinese giant salamander with different treatments: (a) fresh salamander meat; (b)
1001 control; (c) only UV-A; (d) only OG/HP*β*CD NFs; (e) OG/HP*β*CD NFs + UV-A (b-e, 4 ^{o}C, 15
1002 days). The salamander meat was singly sealed with OG/HP*β*CD NFs and irradiated immediately
1003 with UV-A light for 5 min.
1004
1005

2. Results

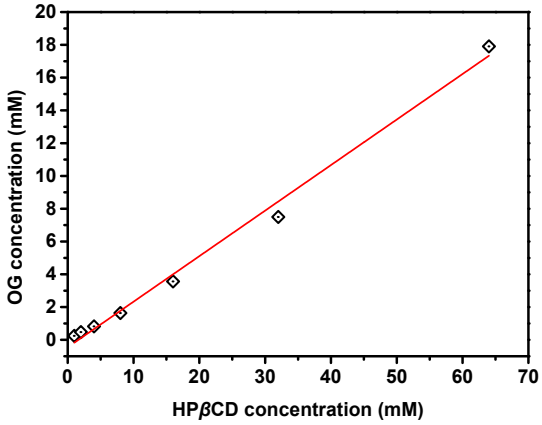

Figure S2. Phase solubility diagrams of OG in aqueous solutions with HPβCD.

In Figure S2, The phase solubility diagram indicated the solubility manner of OG against increasing HPβCD concentrations from 0 to 64 mM. The water solubility of OG was increased over 18 times in the 64 mM concentrated solution of HPβCD after the formation of inclusion complexes. According to the classification of the profile (Higuchi & Connors, 1965), the A-type phase solubility diagram was acquired with different profiles depending on the types of guest molecules and CDs. Among the types of diagram, A_L, A_N and A_P represented liner increases in guest solubility with increasing CDs concentration, positive deviation of linearity and negative deviation of linearity, respectively. In this case, the A_L-type pattern was observed, demonstrating the effect of HPβCD on OG solubility increment was positive at higher concentrations.

Table S1. MIC and MBC of **GA** and **OG** against *E. coli* and *S. aureus* in LB media.

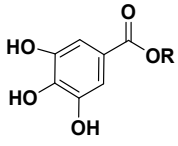	R	*E. coli* (G^-)		*S. aureus* (G^+)		*c*Log *P*[a]
		MIC (mM)	MBC (mM)	MIC (mM)	MBC (mM)	
Gallic acid (**GA**)	H	3.2	6.4	3.2	>6.4	0.4254
Octyl Gallate (**OG**)	C_8H_{17}	0.1	0.2	0.05	0.1	4.6344

[a] Theoretical estimate using ChemBioDraw Ultra 13.0 program. Hydrophobicity of GA and OG from their partition coefficient (Log*P*) analysis. Log*P* is defined as the decadic logarithm of the particular ratio of the concentration of a compound between the two solvents (octanol phase and water phase).

Table S2. Solution Properties and the Fiber Diameters of Resulting Electrospun Nanofibers

Samples	Viscosity (Pa s)	Conductivity (μS cm^{-1})	Average fiber diameter (nm)	Fiber diameter range (nm)
HP*β*CD	1.97±0.05a	15.61±0.35a	981.6±504.3	222-3007
OG/HP*β*CD-IC NFs (1:2)	1.49±0.11b	26.40±0.22b	887.3±355.6	356-2116
OG/HP*β*CD-IC NFs (1:1)	0.97±0.02c	28.01±0.16c	452.6±221.24	141-1352

Significant differences ($p<0.05$) between the groups are denoted by different letters.

1038 **TOC GRAPHIC**

1039

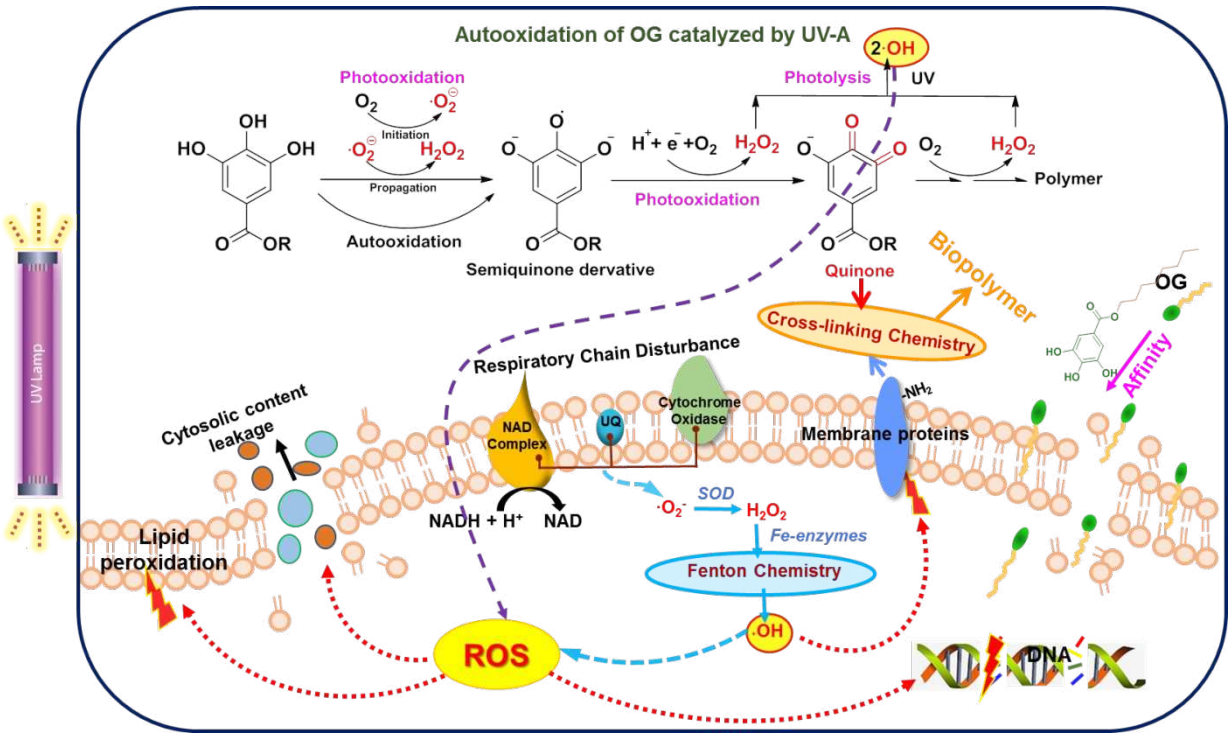

1040

1041

1042